Mathematical Problems in Engineering
Volume 3, pp. 329–371
Reprints available directly from the publisher
Photocopying permitted by license only

Analytical Stability Analysis of Periodic Systems by Poincaré Mappings with Application to Rotorcraft Dynamics

HENRYK FLASHNER* and RAMESH S. GUTTALU

Department of Mechanical Engineering, University of Southern California, Los Angeles, CA 90089-1453, USA

(Received 26 May 1996; Revised 23 May 1997)

A *point mapping* analysis is employed to investigate the stability of periodic systems. The method is applied to simplified rotorcraft models. The proposed approach is based on a procedure to obtain an analytical expression for the period-to-period mapping description of system's dynamics, and its dependence on system's parameters. Analytical stability and bifurcation conditions are then determined and expressed as functional relations between important system parameters. The method is applied to investigate the parametric stability of flapping motion of a rotor and the ground resonance problem encountered in rotorcraft dynamics. It is shown that the proposed approach provides very accurate results when compared with direct numerical results which are assumed to be an "exact solution" for the purpose of this study. It is also demonstrated that the point mapping method yields more accurate results than the widely used classical perturbation analysis. The ability to perform analytical stability studies of systems with multiple degrees-of-freedom is an important feature of the proposed approach since most existing analysis methods are applicable to single degree-of-freedom systems. Stability analysis of higher dimensional systems, such as the ground resonance problems, by perturbation methods is not straightforward, and is usually very cumbersome.

Keywords: Poincaré map; Periodic solutions; Stability; Bifurcation; Rotorcraft

1. INTRODUCTION

Many problems of rotorcraft dynamics are described by differential equations with periodically varying coefficients. This class of systems

* Corresponding author.

is of great theoretical and practical importance because of its many applications in various fields of science and engineering. Stability analysis and bifurcation studies predicting emergence of new periodic solutions while varying system's parameters (bifurcation analysis), are among the most important topics of research for this class of systems.

A variety of analysis methods have been applied to stability analysis of periodic systems. They include Hill's infinite determinant method [21,29], various perturbation methods [22], the averaging methods [4,22,29], and Floquet theory combined with numerical integration [8,11–13,23,27]. It is well established that Hill's method is not convenient for numerical computations. This is because it requires computation of large determinants to determine the transition between stable and unstable regions in the parameter space. Perturbation methods are also limited in application since they are based on expanding the solution in terms of a small parameter that multiplies the periodic terms. When the parameter is not small the accuracy of the solution is very poor. Moreover, increasing the order of approximate solution is usually difficult and does not guarantee uniform convergence to the true solution. Averaging methods are also restricted to systems that possess small parameters and slowly varying amplitudes, and suffer from similar drawbacks in accuracy as those of perturbation methods, see [23]. Several methods have been proposed to study stability of periodic solutions using numerical integration. These methods are based on approximating the periodic function by special functions, for example step functions, Fourier expansion, or Chebyshev polynomials. An alternative integration procedure usually employs various predictor–corrector methods to obtain the transition matrix from which stability conditions are derived numerically. The limitation of this approach is that analytical dependence on parameters is difficult to obtain and, therefore, it is usually not computed. Derivation of parametric dependence requires symbolic inversion of large matrices which is impractical for systems with a large number of degrees-of-freedom (see [27]).

In this paper, a *point mapping* approach is used to derive analytical conditions for stability and bifurcation of periodic equations describing rotorcraft dynamics. The idea of point mapping was first introduced by Poincaré [25]. It is based on expressing system's dynamics in terms of a period-to-period mapping, thus converting the periodic

system into a set of time-invariant discrete-time equations. In the discrete-time representation of the system dynamics, conditions for stability and bifurcation of solutions are expressed in terms of algebraic equations, see [2,18]. The difficulty of applying point mapping method lies in obtaining an analytical expression for the discrete-time representation of a general periodic system. The method of obtaining a point mapping for systems used here was first proposed by Flashner [9], and Flashner and Hsu [10]. The method was modified to include dependence on parameters and applied to the analysis of both autonomous and nonautonomous systems, see [15,16].

In the present study, we use symbolic manipulation to obtain a discrete-time representation of rotorcraft dynamics problems of one and two degrees-of-freedom in an analytical form employing the algorithm given by Flashner and Hsu [10]. The matrix determining the stability characteristics of the system is obtained by matrix multiplication performed symbolically resulting in an analytical expression for the dependence of the matrix on system's parameters. Consequently, analytical expressions for stability and bifurcation can be derived using well-known results for discrete-time systems, see [20]. An advantage of the proposed approach is that the formalism applies equally well to multiple degrees-of-freedom systems for which analytical stability and bifurcation conditions are difficult to derive using other methods of analysis.

The paper is organized as follows. In Section 2, the theory of point mappings, and conditions for stability and bifurcation of periodic solutions of discrete-time systems are presented. The method is applied to study flapping motion of a rotorcraft in Section 4. Stability and bifurcation conditions to various periodic solutions are derived and compared to other methods of solution. In Section 5, stability and bifurcation conditions for a two degrees-of-freedom ground resonance model are derived. Concluding remarks appear in Section 6.

2. POINT MAPPING ANALYSIS

Consider a dynamical system described by a set of N ordinary differential equations

$$\dot{\mathbf{x}}(t) = \mathbf{f}(t, \mathbf{x}(t), \mathbf{s}), \tag{1}$$

where $t \in \mathbf{R}^+$ denotes time, $\mathbf{x} \in \mathbf{R}^N$ is the state vector, $\mathbf{s} \in \mathbf{R}^L$ is a parameter vector, and $\mathbf{f}: \mathbf{R}^+ \times \mathbf{R}^N \times \mathbf{R}^L \to \mathbf{R}^N$ is analytic in the components of $\mathbf{x}$ and of $\mathbf{s}$. In addition, $\mathbf{f}$ is periodic in t with period T, i.e. $\mathbf{f}(t, \mathbf{x}(t), \mathbf{s}) = \mathbf{f}(t+T, \mathbf{x}(t), \mathbf{s})$. Define the dynamic relationship between the state of the system at the beginning of a period to the state at the end of the same period. This relationship is given by a set of difference equations, called a *point mapping* or the *Poincaré map*, expressed as follows

$$\mathbf{x}_{n+1} = \mathbf{G}(\mathbf{x}_n, \mathbf{s}), \tag{2}$$

where $\mathbf{x}_{n+1}$ and $\mathbf{x}_n$ are the states of the system at $t=(n+1)T$ and $t=nT$, respectively. Note that since $\mathbf{f}$ is analytic, the equations in (1) satisfy Lipschitz conditions and therefore $\mathbf{G}$ is one to one for a fixed value of $\mathbf{s}$.

2.1. Periodic Solutions

Given a fixed parameter vector $\mathbf{s} \in \mathbf{S}^*$, a periodic solution of period KT, $K \in \mathbf{Z}^+$, of the dynamical system (1) is given by the function $\mathbf{x}^*(t; \mathbf{s}): \mathbf{R}^+ \to \mathbf{R}^N$ satisfying the following equations:

$$\begin{aligned} \dot{\mathbf{x}}^*(t; \mathbf{s}) &= \mathbf{f}(t, \mathbf{x}^*(t; \mathbf{s}), \mathbf{s}) \quad \forall t \geq 0, \\ \mathbf{x}^*(t; \mathbf{s}) &= \mathbf{x}^*(t + KT; \mathbf{s}). \end{aligned} \tag{3}$$

Define $\mathbf{z}(t) = \mathbf{x}(t) - \mathbf{x}^*(t; \mathbf{s})$ as the perturbation of the state $\mathbf{x}$ about the periodic solution $\mathbf{x}^*$. Then, the equations of motion (1) can be written as

$$\begin{aligned} \dot{\mathbf{z}}(t) &= \mathbf{f}(t, \mathbf{z}(t), \mathbf{s}; \mathbf{x}^*) \\ &= \mathbf{A}(t, \mathbf{s})\mathbf{z}(t) + \sum_{k=2}^{\infty} \mathbf{r}_k(t, \mathbf{z}(t), \mathbf{s}; \mathbf{x}^*), \end{aligned} \tag{4}$$

where the matrix $\mathbf{A}(t) \in \mathbf{R}^{N \times N}$ is given by

$$\mathbf{A}(t, \mathbf{s}) = \left[\frac{\partial \mathbf{f}(t, \mathbf{x}, \mathbf{s})}{\partial \mathbf{x}} \right]_{\mathbf{x}=\mathbf{x}^*} \tag{5}$$

and $\mathbf{r}_k(t, \mathbf{z}(t), \mathbf{s}; \mathbf{x}^*)$ is a vector of all polynomials of degree k in the components of $\mathbf{z}(t)$. It is clear that $\mathbf{A}(t)$ is periodic in t of period KT.

In order to analyze these periodic solutions using point mappings, the notion of a *P-K solution* is employed. A *P-K* solution of the point mapping (2) for some $\mathbf{s} \in \mathbf{S}^* \in \mathbf{R}^L$, consists of K distinct points $\mathbf{x}_j^*(\mathbf{s})$, $j = 1, 2, \ldots, K$, such that

$$\begin{aligned} \mathbf{x}_{j+1}^*(\mathbf{s}) &= \mathbf{G}(\mathbf{x}_j(\mathbf{s}), \mathbf{s}), \quad j = 1, 2, \ldots, K-1, \\ \mathbf{x}_1^*(\mathbf{s}) &= \mathbf{G}(\mathbf{x}_K^*(\mathbf{s}), \mathbf{s}). \end{aligned} \tag{6}$$

It is assumed that *P-K* solutions satisfying (6) exists $\forall \mathbf{s} \in \mathbf{S}^*$. Finding a *P-K* solution of a point mapping in Eq. (2) is equivalent to finding a periodic solution of the corresponding continuous-time system in Eq. (1) that satisfies Eq. (3). It should also be noted that, *provided* one can determine the point map $\mathbf{G}(\mathbf{x}, \mathbf{s})$, finding a *P-K* solution requires solving a set of N algebraic equations in N unknowns given in Eq. (6). This is in contrast to finding periodic solutions using the original continuous-time description which requires a search for a time-dependent function $\mathbf{x}^*(t; \mathbf{s})$ in the space of periodic functions. Note also that an equilibrium point $\mathbf{x}^*$ of (1), i.e. a point that satisfies $\mathbf{f}(t, \mathbf{x}^*, \mathbf{s}^*) = 0$ for all $t > t^*$, $t^* \in \mathbf{R}^+$, is clearly a *P*-1 solution of the corresponding point mapping (2).

As in the case of continuous time equations, the point mapping (2) can be expressed as a perturbation about a given periodic solution. Let $\mathbf{x}_j^*$ be a point that belongs to a *P-K* solution. Then, Eq. (2) can be written as

$$\mathbf{z}_{m+1} = \mathbf{H}(\mathbf{s})\mathbf{z}_m + \sum_{i=2}^{\infty} \mathbf{q}_i(\mathbf{z}_m, \mathbf{s}; \mathbf{x}_j^*), \quad m = 1, 2, \ldots \tag{7}$$

where $\mathbf{z}_m = \mathbf{x}((K+m)T) - \mathbf{x}_j^*$ and $\mathbf{q}_i(\mathbf{z}_m, \mathbf{s}; \mathbf{x}_j^*)$ is a vector of all polynomials of degree i in the components of $\mathbf{z}_m$. The matrix $\mathbf{H}(\mathbf{s}) \in \mathbf{R}^{N \times N}$ is given by

$$\mathbf{H}(\mathbf{s}) = \mathbf{H}_K(\mathbf{s})\mathbf{H}_{K-1}(\mathbf{s})\mathbf{H}_{K-2}(\mathbf{s}) \cdots \mathbf{H}_1(\mathbf{s}), \tag{8}$$

where

$$\mathbf{H}_j(\mathbf{s}) = \left[\frac{\partial \mathbf{G}(\mathbf{x}, \mathbf{s})}{\partial \mathbf{x}}\right]_{\mathbf{x}=\mathbf{x}_j^*}. \tag{9}$$

2.2. Stability and Bifurcation Conditions

Stability of a *P-K* solution can be expressed in terms of the eigenvalues $\lambda_i(\mathbf{H}(\mathbf{s}))$, $i=1,\ldots,N$, of the matrix $\mathbf{H}(\mathbf{s})$ as follows:

(a) A *P-K* solution of (2) is *asymptotically stable* if and only if

$$|\lambda_i(\mathbf{H}(\mathbf{s}))| < 1, \quad \text{for all } i,\ i=1,\ldots,N. \tag{10}$$

(b) A *P-K* solution of (2) is *unstable* if

$$|\lambda_i(\mathbf{H}(\mathbf{s}))| > 1, \quad \text{for some } i,\ i=1,\ldots,N. \tag{11}$$

(c) Linear stability analysis is *inconclusive* if

$$|\lambda_i(\mathbf{H}(\mathbf{s}))| = 1, \quad \text{for some } i,\ i=1,\ldots,N. \tag{12}$$

Let condition (12) be satisfied for some $\mathbf{s}=\mathbf{s}_0$. If, in addition,

$$\left[\frac{\mathrm{d}}{\mathrm{d}\mathbf{s}}|\lambda_i(\mathbf{H}(\mathbf{s}))|\right]_{\mathbf{s}=\mathbf{s}_0} > 0 \tag{13}$$

holds, then the given *P-K* solution looses stability.

From implicit function theorem, it follows that if for some $\mathbf{s} \in \mathbf{S}$ there exists an integer M such that

$$\det(\mathbf{I} - \mathbf{H}^M(\mathbf{s})) = 0, \tag{14}$$

then a bifurcation of a *P-K* solution to a *P-MK* solution may occur. Equivalently, a bifurcation from a *P-K* solution to a *P-MK* solution may occur if for some i, $i=1,2,\ldots,N$,

$$|\lambda_i(\mathbf{H}(\mathbf{s}))|^M = 1, \tag{15}$$

where λ_i is an eigenvalue of $\mathbf{H}(\mathbf{s})$.

Using Eq. (14), the following conditions are obtained:

(a) Bifurcation of *P-K* $\rightarrow$ *P-K*:

$$\det(\mathbf{I} - \mathbf{H}) = 0. \tag{16}$$

(b) Bifurcation of $P\text{-}K \rightarrow P\text{-}2K$:

$$\det(\mathbf{I}+\mathbf{H}) = 0. \tag{17}$$

(c) Bifurcation of $P\text{-}K \rightarrow P\text{-}MK$:

$$\begin{aligned} &\det(\mathbf{I}+\mathbf{H}^{M/2}) = 0, && M \text{ even, } M/2 \text{ even,} \\ &\det(\mathbf{I}-\mathbf{H}+\mathbf{H}^2-\mathbf{H}^3\cdots+\mathbf{H}^{(M/2)-1}) = 0, && M \text{ even, } M/2 \text{ odd,} \\ &\det(\mathbf{I}+\mathbf{H}+\mathbf{H}^2+\mathbf{H}^3\cdots+\mathbf{H}^{M-1}) = 0, && M \text{ odd.} \end{aligned} \tag{18}$$

It should be noted that for two-dimensional Hamiltonian systems ($N=2$), Eq. (14) is satisfied for all t. Therefore, a $P\text{-}K$ solution cannot loose stability via bifurcations to $P\text{-}MK$ solutions with $M>2$. The mechanism of stability loss for Hamiltonian systems is only via bifurcations to a new $P\text{-}K$ or to a $P\text{-}2K$ solutions.

3. DERIVATION OF POINT MAPPING REPRESENTATION OF SYSTEM DYNAMICS

The procedure to obtain approximate point mappings used in this study was first introduced by Flashner [9] and Flashner and Hsu [10]. For a modification of this procedure see [15]. The underlying philosophy and the proposed procedure are presented in the following.

3.1. Jets and Truncation Operation

Since the function $\mathbf{f}(t, \mathbf{x}(t), \mathbf{s})$ is analytic, it can be expressed by a series of the form

$$\mathbf{f}(t,\mathbf{x},\mathbf{s}) = \mathbf{p}(t,\mathbf{x},\mathbf{s}) = \sum^{p} b^{(f)}_{i_1\cdots i_n}(t) x_{i_1}\cdots x_{i_n}, \tag{19}$$

where $\mathbf{p}(t,\mathbf{x},\mathbf{s})$ denotes a vector homogeneous polynomial of degree P in the state variables x_i, $i=1,2,\ldots,N$. The symbol $\sum^{P}$ denotes summation over all sequences $i_1,\ldots,i_r$ with $0\le i_j\le N$ for each j,

$\sum_{j=1}^{r} i_j = r$ and $r = 1, 2, \ldots, N$. In other words, a homogeneous polynomial of degree P contains terms with sum of the powers of x_i (for $i = 1, 2, \ldots, N$) less than or equal to P. To abbreviate notation, denote this set of indices $i_1, \ldots, i_r$ by E_r. Then we denote the coefficients of the homogeneous polynomial in Eq. (19) by the symbol $b_{E_r}^{(f)}(t)$. These coefficients, in general, can be functions of the parameter vector $\mathbf{s}$.

The numerical algorithm for obtaining a point map is based on approximating polynomial functions by truncating at some degree k. Let $\mathbf{p}(t, \mathbf{x})$ be a polynomial of degree greater than k. Define the truncation operation at degree k denoted by

$$\mathbf{p}_k(t, x) = \overline{\mathbf{p}(t, \mathbf{x})}^k = \sum^k b_{E_r}(t) x_{i_1} \cdots x_{i_r} \tag{20}$$

to be the polynomial formed by taking only those terms whose degree is k or less. Let $\mathbf{p}(t, \mathbf{x})$ and $\mathbf{q}(t, \mathbf{x})$ be two vector polynomials, then the truncation operation obeys the following rules (Poston and Stewart [26]):

$$\overline{\mathbf{p} + \mathbf{q}}^k = \overline{\mathbf{p}}^k + \overline{\mathbf{q}}^k, \tag{21}$$

$$\overline{\mathbf{p} \cdot \mathbf{q}}^k = \overline{\overline{\mathbf{p}}^k \cdot \overline{\mathbf{q}}^k}^k. \tag{22}$$

If $\mathbf{q}(t, \mathbf{x})$ does not contain terms that are free of the components of $\mathbf{x}$ then

$$\overline{\mathbf{p}(t, \mathbf{q}(t, \mathbf{x}))}^k = \overline{\overline{\mathbf{p}}^k(\overline{\mathbf{q}}^k(t, \mathbf{x}))}^k. \tag{23}$$

If the function $\mathbf{f}(t, \mathbf{x}, \mathbf{s})$ is not a finite order polynomial but is analytic for all $\mathbf{x}$ (and for a given $\mathbf{s}$), it can be represented by a Taylor series as an infinite polynomial ($P \to \infty$ in (19)). In this case $\mathbf{f}(t, \mathbf{x}, \mathbf{s})$ can be approximated by a k-jet denoted by $j^k\mathbf{f}$, that is, by a Taylor series expansion about a point $\mathbf{x}_0$ truncated at degree k. In terms of this truncation notation we can express the k-jet's behavior with respect to sums, products and composition (the jet analog of the chain rule). For analytic vector functions $\mathbf{p}(t, \mathbf{x})$ and $\mathbf{q}(t, \mathbf{x})$, the

following equalities hold (Poston and Stewart [26]):

$$j^k(\mathbf{p}+\mathbf{q}) = j^k\mathbf{p} + j^k\mathbf{q}, \tag{24}$$

$$j^k(\mathbf{p} * \mathbf{q}) = \overline{j^k\mathbf{p} * j^k\mathbf{q}}^k, \tag{25}$$

$$j^k(\mathbf{p} \circ \mathbf{q}) = \overline{j^k\mathbf{p} \circ j^k\mathbf{q}}^k. \tag{26}$$

3.2. Computation of Point Mappings

The computational algorithm for evaluating a point mapping is based on the fact that the operations of truncation and telescoping on polynomials can be interchanged. Moreover, the Runge–Kutta method of integration can be expressed as a sequence of polynomial telescoping and truncation operations which finally results in a truncated polynomial expression for the point mapping $\mathbf{G}(\mathbf{x}, \mathbf{s})$ of Eq. (2).

To integrate Eq. (1), the algorithm uses the Runge–Kutta method which can be formulated as follows (see Shampine [28]):

$$\mathbf{x}(t_p + h) = \mathbf{x}(t_p) + h\sum_{m=1}^{M} d_m \mathbf{k}_m(t, \mathbf{x}), \tag{27}$$

where M is the order of the Runge–Kutta method, h is the time step, and d_m are certain constants determined by the Runge–Kutta method. The vectors $\mathbf{k}_m$ for the differential Eqs. (1) are given by

$$\mathbf{k}_m(t, \mathbf{x}) = \mathbf{f}(t_p + ha_m, \mathbf{x}(t_p) + c_m\mathbf{k}_{m-1}, \mathbf{s}), \quad m = 1, 2, \ldots, M. \tag{28}$$

The constants a_m and c_m are given by the particular Runge–Kutta method to be used with $a_1 = 0$ and $c_1 = 0$.

To derive the algorithm, the period T is divided into N_t subintervals of length $h = T/N_t$. We are interested in computing a k-jet of the point mapping $\mathbf{G}$ in (2). Let $m = 1$ in Eq. (27) and let $\mathbf{x}(t_p) = \mathbf{x}(nT + (i-1)h) = \mathbf{x}$ with $1 \le i \le N_t$. If $\mathbf{f}(t, \mathbf{x}, \mathbf{s})$ is vector polynomial in $\mathbf{x}$ given by (19) (possibly with $P \to \infty$), then the k-jet of

the function $\mathbf{k}_1(t, \mathbf{x})$ is given by

$$j^k\mathbf{k}_1(i;\mathbf{x}) = \sum^{k} {}^{(i)}b^{(1)}_{E_r}\mathbf{x}_{i_1}\cdots\mathbf{x}_{i_r} = \mathbf{p}^1_k(i;\mathbf{x}), \tag{29}$$

where

$${}^{(i)}b^{(1)}_{E_r} = \begin{cases} {}^{(1)}\beta^{(f)}_{E_r} & i = 1; \qquad r = 1,2,\ldots,k, \\ {}^{(i)}\beta_{E_r} & i = 2,\ldots,N_t; \quad r = 1,2,\ldots,k. \end{cases} \tag{30}$$

The coefficients ${}^{(i)}\beta_{E_r}$ are defined in Eq. (36). The vector $\mathbf{p}^1_k(i;\mathbf{x})$ is a homogeneous vector polynomial of degree k. To evaluate the k-jets of $\mathbf{k}_m$, $m = 2, 3, \ldots, M$, we note that

$$\begin{aligned} \mathbf{x}(t_p) + c_m{}^{(i)}\mathbf{k}_{m-1}(i;\mathbf{x}) &= \sum^{k} {}^{(i)}\alpha^{(m)}_{E_r}\mathbf{x}_{i_1}\cdots\mathbf{x}_{i_r} \\ &= \mathbf{r}^m_k(i;\mathbf{x}), \quad m = 2,3,\ldots,M, \end{aligned} \tag{31}$$

where

$${}^{(i)}\alpha^{(m)}_{E_r} = \begin{cases} c^{(i)}_m b^{(m-1)}_{E_r}, & r \neq 1, \\ e_{i_r} + c^{(i)}_m b^{(m-1)}_{E_r}, & r = 1; \quad i_r = 1,2,\ldots,N \end{cases} \tag{32}$$

and

$$e_{i_r} = [0 \;\; 0 \;\; \cdots \;\; 0 \;\; 1 \;\; 0 \;\; \cdots \;\; 0 \;\; 0]^{\mathrm{T}}, \tag{33}$$

where e_{i_r} is a column vector such that all of its entries are zero except the i_rth entry which is one. Here, $\mathbf{r}^m_k(i;\mathbf{x})$ denotes a homogeneous vector polynomial of degree k. Using Eq. (28) and identity (26), we have

$$\begin{aligned} j^k\mathbf{k}_m(i;x) &= \overline{j^k\mathbf{f}((i-1)h + ha_m, \mathbf{r}^m_k(i;x))}^{\,k} \\ &= \overline{\mathbf{p}(\mathbf{r}^m_k(i;\mathbf{x}))}^{\,k} \\ &= \sum^{k} {}^{(i)}b^{(m)}_{E_r}x_{i_1}\cdots x_{i_N} \\ &= \mathbf{p}^m_k(i;\mathbf{x}). \end{aligned} \tag{34}$$

Evaluation of the coefficients ${}^{(i)}b_{E_r}^{(m)}$ involves 'telescoping' of polynomials. This can be done in many different ways, for example, by using the multinomial theorem (see Flashner and Hsu [10]). The 'telescoping' operation can be carried out by using only one procedure that performs multiplication of two scalar polynomials. This approach is very efficient computationally and allows inclusion of parameter dependence. It also gives sufficient freedom to allow various truncation schemes to be explained later. To evaluate the k-jet at $t = nT + h$, consider Eq. (27) and observe that

$$j^k\mathbf{x}(t_p + ih) = \mathbf{x} + \sum_{m=1}^{M} h d_m \mathbf{p}_k^m(i; \mathbf{x}) = \sum^{k} {}^{(i)}\beta_{E_r} x_{i_1} \cdots x_{i_N} = \mathbf{Q}_k(i; \mathbf{x}), \tag{35}$$

where $\mathbf{Q}_k(i; \mathbf{x})$ is a k-degree vector polynomial whose coefficients are given by

$${}^{(i)}\beta_{E_r} = \begin{cases} h \sum_{m=1}^{M} d_m \, {}^{(i)}b_{E_r}^{(m)}, & r \neq 1, \\ e_{i_r} + h \sum_{m=1}^{M} d_m \, {}^{(i)}b_{E_r}^{(m)}, & r = 1; \ i_r = 1, 2, \ldots, N. \end{cases} \tag{36}$$

Using the relations given in Eqs. (29)–(34) and (36) one can calculate the coefficients ${}^{(i)}\beta_{E_r}$ in terms of the coefficients ${}^{(i)}b_{E_r}^{(f)}$ of k-jet of differential equation given in (19). Substitution of these coefficients in (35) results in the k-jet approximation of a point mapping over the time interval h.

Computation of the coefficients of a k-jet of the point mapping over the period T is done by repeating $(N_t - 1)$ times the sequence given in Eqs. (29)–(36) to get

$$\begin{aligned} \mathbf{x}((n+1)T) &= \overline{\mathbf{Q}_k(N_t; (\mathbf{Q}_k(N_t - 1; (\mathbf{Q}_k(N_t - 2; (\cdots \mathbf{Q}_k(1; (\mathbf{Q}_k(0; \mathbf{x}))}^{k} \\ &= \sum^{k} \gamma_{E_r} x_{i_1} \cdots x_{i_r} \\ &= j^k \mathbf{G}(\mathbf{x}, \mathbf{s}), \end{aligned} \tag{37}$$

where $\mathbf{Q}_k(0; \mathbf{x}) = \mathbf{x}$. As in computation of the coefficients of the mapping $\mathbf{Q}_k(i; \mathbf{x})$, evaluation of the coefficients γ_{E_r} involves 'telescoping' of polynomials. Therefore, the same algorithm of evaluating the coefficients used in Eq. (34) can be employed here.

In summary, the numerical algorithm for computing coefficients of the vector polynomial for the point map involves the following steps:

(i) Divide the period T into N_t subintervals of length h and set $i=1$. Choose P, the order of polynomial truncation required.
(ii) Compute the coefficients ${}^{(i)}b_{E_r}^{(1)}$ for $r=1,2,\ldots,P$ using Eq. (30).
(iii) For $m=2,3,\ldots,M$:
  (a) Compute the coefficients ${}^{(i)}\alpha_{E_r}^{(m)}$ for $r=1,2,\ldots,P$ using Eq. (32).
  (b) Compute the coefficients ${}^{(i)}b_{E_r}^{(m)}$ for $r=1,2,\ldots,P$ according to Eq. (34) using the telescoping algorithm.
(iv) Compute the coefficients ${}^{(i)}\beta_{E_r}$ for $r=1,2,\ldots,P$ using Eq. (36).
(v) Compute the coefficients ${}^{(i)}\gamma_{E_r}$ of the expression

$$\mathbf{Q}_k(i;\mathbf{Q}_k(i-1;\mathbf{x}))=\sum^{P}{}^{(i)}\gamma_{E_r}\, x_{i_1}\cdots x_{i_r}. \tag{38}$$

The computation of these coefficients is done using the telescoping algorithm used in (iii).
(vi) If $i=N_t$, $\gamma_{E_r}={}^{(i)}\gamma_{E_r}$, stop. Otherwise, set $i=i+1$ and repeat steps (ii)–(v).

3.3. Dependence on Parameters

The algorithm devised here can separately keep track of the powers of the components of the parameter vector **s** and state vector **x**. We assume that the coefficients of the polynomial given in Eq. (19) consist of powers of the components of the vector **s**. Alternatively, we can assume that these coefficients are analytic functions of the components of **s** and then we can take the p-jet of the coefficients with respect to the powers of s_j, $j=1,2,\ldots,L$, as follows:

$$b_{E_r}^{(f)}(t)=\sum_{q}^{p}\sigma_{E_r}(t)s_{j_1}\cdots s_{j_L}, \tag{39}$$

where the symbol $\sum_q^p$ denotes summation over all sequences $j_1,\ldots,j_L$ with $0\le j_\nu\le L$ for each ν, $\sum_{\nu=1}^{L}=q$, and $q=1,2,\ldots,p$. In

short, we define the coefficients of the function $\mathbf{f}(t, \cdot, \cdot)$ in set notation as $\sigma_{E_r, E_q}(t)$. Using this notation convention, the k-jet in the components of $\mathbf{x}$ and $\mathbf{p}$-jet in the components of $\mathbf{s}$ for the given system can be written as

$$j_x^k j_s^p = \sum_r^k \sum_q^p \sigma_{E_r, E_q}(t) x_{i_1} \cdots x_{i_N} \, s_{j_1} \cdots s_{j_L}. \tag{40}$$

In order to keep track of the powers of the components of $\mathbf{x}$ and in order to perform the appropriate truncation with respect to $\mathbf{s}$, the polynomial telescoping routine is only slightly modified. Since telescoping in the proposed algorithms is performed by simple multiplication, an internal multiplication scheme operating on the powers of $\mathbf{s}$ is implemented and appropriate truncation is performed. As explained before, in perturbation analysis the truncation on the parameters is carried out up to low order. Therefore, separate truncation of parameter powers significantly speeds up computation.

3.4. Point Mappings of Linear Systems

As stated before, the conditions for stability and bifurcation depend only on the linear terms of the point mapping (7) (that is, on the matrix $\mathbf{H}(\mathbf{s})$). Noting that the two properties of the point mapping $\mathbf{G}_p$ mentioned above, namely, (a) the operations of polynomial truncation and telescoping can be interchanged, and (b) the lowest order polynomial in (4) is of degree one, and that there is no term on the right hand side of Eq. (4) that is not a function of the elements of the state vector $\mathbf{z}$, then for stability analysis it is sufficient to obtain the point mapping of the linearized system:

$$\dot{\mathbf{z}}(t) = \mathbf{A}(t, \mathbf{s})\mathbf{z}(t). \tag{41}$$

Using (28), for the system in Eq. (41), it can be shown that the vectors $\mathbf{k}_m$ are given by

$$\mathbf{k}_m = \left[\mathbf{A}(t_p + ha_m, \mathbf{s}) + \sum_{l=1}^{m} \prod_{i=2}^{l} hc_i \mathbf{A}(t_p + ha_{i-1}, \mathbf{s})\right] \mathbf{z}(t_p).$$

Using (27), we obtain the following:

$$\mathbf{z}(t_{p+1}) = \Phi(t_p, \mathbf{s})\mathbf{z}(t_p), \tag{42}$$

where

$$\Phi(t_p, \mathbf{s}) = \mathbf{I} + h\sum_{m=1}^{R}\left[d_m\mathbf{A}(t_p + ha_m, \mathbf{s}) + \sum_{l=1}^{m}\prod_{i=2}^{l} hc_i\mathbf{A}(t_p + ha_{i-1}, \mathbf{s})\right]. \tag{43}$$

Dividing the period KT (with K and T given) into N_t intervals and successively applying (42) by using $p = 0, \ldots, N_t$, yields

$$\mathbf{z}(t_0 + KT) = \left\{\prod_{p=1}^{N_t}\Phi(t_p, \mathbf{s})\right\}\mathbf{z}(t_0). \tag{44}$$

Using Eqs. (43) and (44) results in the following expression for the matrix $\mathbf{H}(\mathbf{s})$:

$$\begin{aligned}\mathbf{H}(\mathbf{s}) &= \prod_{p=1}^{N_t}\Phi(t_p, \mathbf{s}) \\ &= \prod_{p=1}^{N_t}\left\{\mathbf{I} + h\sum_{m=1}^{R} d_m\left[\mathbf{A}(t_p + ha_m, \mathbf{s}) + \sum_{l=1}^{m}\prod_{i=2}^{l} hc_i\mathbf{A}(t_p + ha_{i-1}, \mathbf{s})\right]\right\}.\end{aligned} \tag{45}$$

Note that Eq. (45) involves only multiplications and additions of the matrix $\mathbf{A}(t, \mathbf{s})$ evaluated at different time instances. Collecting powers of the components of $\mathbf{s}$ for every element of $\mathbf{H}(\mathbf{s})$ and truncating at a required power P yields a matrix $\mathbf{H}_P(\mathbf{s})$ in which every element consists of homogeneous polynomials of the elements of $\mathbf{s}$ up to order P.

The algorithm for point mapping has been implemented using the symbolic algebra packages REDUCE and MATHEMATICA, and a specially developed FORTRAN program to perform symbolic vector polynomial operations. The point mappings for the rotorcraft problems were derived using both the REDUCE program and FORTRAN. The same programs were used to obtain analytical expressions for bifurcation conditions by evaluating Eqs. (16)–(18).

4. PARAMETRIC STABILITY OF FLAPPING MOTION OF A ROTOR

The differential equation of flapping motion of single gimballed rotor blade or of a two-bladed teetering rotor may be approximated by

$$\frac{d^2\beta}{d^2\phi}+\frac{\gamma}{8}\left(1+\frac{4\rho\mu}{3}\sin\phi\right)\frac{d\beta}{d\phi}+\left[\omega_0^2+\frac{\gamma\mu}{8}\left(\mu\sin 2\phi+\frac{4\rho}{3}\cos\phi\right)\right]\beta=0, \tag{46}$$

where β represents the blade flap angle, ϕ is the azimuth angle of the blade, μ is the blade advance ratio, γ is the Lock number for the flow, ω_0 is the natural frequency of the system, and $\rho=1$ for a gimballed rotor, and $\rho=0$ for a teetering rotor (see Johnson [19]). In state-space form with vector $\mathbf{x}=[\beta,\dot{\beta}]^T$, we have

$$\dot{\mathbf{x}}=\mathbf{A}(\phi)\mathbf{x},\ \mathbf{A}(\phi+T)=\mathbf{A}(\phi),\quad T=2\pi, \tag{47}$$

$$\mathbf{A}(\phi)=\begin{bmatrix}0 & 1\\ -\omega_0^2-\frac{\gamma\mu}{8}\left(\mu\sin 2\phi+\frac{4\rho}{3}\cos\phi\right) & -\frac{\gamma}{8}\left(1+\frac{4\rho\mu}{3}\sin\phi\right)\end{bmatrix}, \tag{48}$$

where the superposed dot represents the derivative. Since the system is linear in the state variable $\mathbf{x}$, it follows from the discussion in Section 3 that the corresponding point mapping $\mathbf{G}$ is also linear in $\mathbf{x}$ but depends in a nonlinear way on the parameters ω_0, μ and γ. For a given value of ρ, the point mapping can be expressed as follows:

$$\mathbf{x}(n+1)=\mathbf{G}(\mathbf{x}(n);\ \omega_0,\mu,\gamma)=\mathbf{H}(\omega_0,\mu,\gamma)\mathbf{x}(n),\quad n=1,2,\ldots \tag{49}$$

The approach for obtaining the truncated point mapping introduced in Section 3 was used to evaluate the matrix $\mathbf{H}(\omega_0,\mu,\gamma)$ using Eq. (45). Two separate cases of $\rho=0$ and $\rho=1$ are considered below. For each case fixing $P=50$, coefficients of the various powers of $\omega_0^{2i}\mu^j\gamma^k$, $i+j+k\le P$, $i=0,1,2,\ldots,P$, $j=0,1,2,\ldots,P$, $k=0,1,2,\ldots,P$, in the elements of the matrix $\mathbf{H}$ were obtained, with $K=1$, $t_0=0$, $T=2\pi$, $N_t=100$, resulting in a time step of $h=2\pi/100$. The result is a matrix $\mathbf{H}(\omega_0,\mu,\gamma)$ whose elements are homogeneous polynomials in ω_0, μ and γ, order $P=50$, and the matrix $\mathbf{H}_P$ is said to be of order $\mathcal{O}(\omega_0^{2P}\mu^P\gamma^P)$.

4.1. Teetering Rotor ($\rho = 0$)

For ease of presentation, the coefficients of each term in $\mathbf{H}(\omega_0, \mu, \gamma)$ are identified as rational fractions of powers of π. Let H_{ij} be the components of the matrix $\mathbf{H}$. The resulting leading coefficients of the matrix are

$$
\begin{aligned}
H_{11} &= 1 - \left(\frac{15\pi^2\gamma}{377} - \frac{\pi^3\gamma^2}{201}\right)\mu^2 \\
&\quad - \left(2\pi^2 - \frac{\pi^3\gamma}{6} + \frac{\pi^4\gamma^2}{96} - \frac{\pi^5\gamma^3}{1920} - \frac{11\pi^4\gamma\mu^2}{489}\right)\omega_0^2 \\
&\quad + \left(\frac{2\pi^4}{3} - \frac{\pi^5\gamma}{15} + \frac{\pi^6\gamma^2}{240}\right)\omega_0^4 - \left(\frac{4\pi^6}{45} - \frac{\pi^7\gamma}{105}\right)\omega_0^6 + \frac{2\pi^8\omega_0^8}{315} + \cdots \\
H_{12} &= 2\pi - \frac{\pi^2\gamma}{4} + \frac{\pi^3\gamma^2}{48} - \frac{\pi^4\gamma^3}{768} + \frac{\pi^5\gamma^4}{15360} \\
&\quad - \left(\frac{4\pi^3}{3} - \frac{\pi^4\gamma}{6} + \frac{\pi^5\gamma^2}{80} - \frac{\pi^6\gamma^3}{1440}\right)\omega_0^2 \\
&\quad + \left(\frac{4\pi^5}{15} - \frac{\pi^6\gamma}{30} + \frac{\pi^7\gamma^2}{420}\right)\omega_0^4 - \left(\frac{8\pi^7}{315} - \frac{\pi^8\gamma}{315}\right)\omega_0^6 + \frac{\pi^9\omega_0^8}{709} + \cdots \\
H_{21} &= \frac{\pi^2\gamma^2\mu^2}{201} - \left(2\pi - \frac{\pi^2\gamma}{4} + \frac{\pi^3\gamma^2}{48} - \frac{\pi^4\gamma^3}{768}\right)\omega_0^2 \\
&\quad + \left(\frac{4\pi^3}{3} - \frac{\pi^4\gamma}{6} + \frac{\pi^5\gamma^2}{80}\right)\omega_0^4 - \left(\frac{4\pi^5}{15} - \frac{\pi^6\gamma}{30}\right)\omega_0^6 + \frac{8\pi^7\omega_0^8}{315} + \cdots \\
H_{22} &= 1 - \frac{\pi\gamma}{4} + \frac{\pi^2\gamma^2}{32} - \frac{\pi^3\gamma^3}{384} + \frac{\pi^4\gamma^4}{6144} + \left(\frac{15\pi^2\gamma}{377} - \frac{\pi^3\gamma^2}{201}\right)\mu^2 \\
&\quad - \left(2\pi^2 - \frac{\pi^3\gamma}{3} + \frac{\pi^4\gamma^2}{32} - \frac{\pi^5\gamma^3}{480} + \frac{11\pi^4\gamma\mu^2}{489}\right)\omega_0^2 \\
&\quad + \left(\frac{2\pi^4}{3} - \frac{\pi^5\gamma}{10} + \frac{\pi^6\gamma^2}{120}\right)\omega_0^4 \\
&\quad - \left(\frac{4\pi^6}{45} - \frac{4\pi^7\gamma}{315}\right)\omega_0^6 + \frac{2\pi^8\omega_0^8}{315} + \cdots
\end{aligned}
\tag{50}
$$

It is seen from the expressions in (50) that higher order terms of $\mathbf{H}$ possess considerably smaller magnitude of coefficients. In order to assess the accuracy of the point mapping expression, we consider the

determinant of **H**, a closed-form expression for which is readily known for this example.

Undamped case ($\gamma = 0$) For this case, the dynamical system given by (47) is Hamiltonian (or area-preserving) and therefore, $\det \mathbf{H}(\omega_0, \mu, 0) = 1$. Evaluating the determinant of **H** given by (50), we obtain

$$\begin{aligned}\det \mathbf{H}(\omega_0, \mu, 0) = 1 &- 8.89 \times 10^{-11}(\pi\omega_0)^6 + 4.44 \times 10^{-15}(\pi\omega_0)^8 \\ &+ 3.91 \times 10^{-21}(\pi\omega_0)^{12} - 3.91 \times 10^{-25}(\pi\omega_0)^{14} \\ &+ 9.76 \times 10^{-30}(\pi\omega_0)^{16} \\ &- 1.15 \times 10^{-31}(\pi\omega_0)^{18} + \cdots \end{aligned} \tag{51}$$

Observe that in (51), only the parameters ω_0 appears and all the terms have negligible coefficients which decrease with increasing powers of ω_0. The magnitude of these coefficients depends primarily on the size of time step h. For example, when h is reduced by half, determinant of **H** contains only the following five terms:

$$\begin{aligned}\det \mathbf{H}(\omega_0, \mu, 0) = 1 &- 2.78 \times 10^{-12}(\pi\omega_0)^6 + 3.47 \times 10^{-17}(\pi\omega_0)^8 \\ &+ 3.84 \times 10^{-24}(\pi\omega_0)^{12} - 9.62 \times 10^{-29}(\pi\omega_0)^{14}. \end{aligned} \tag{52}$$

It is observed that by decreasing time step h, the magnitude of the coefficients of all the powers of ω_0 in (51) consistently decreases implying that they tend to zero as $h \to 0$. Hence, $\det \mathbf{H}(\omega_0, \mu, 0) \to 1$ as $h \to 0$ in Eq. (51).

Damped case ($\gamma \neq 0$) Using Liouville theorem, the closed-form expression for determinant of **H**, denoted by $\det \mathbf{H}_E$, is (see Arnold [1])

$$\begin{aligned}\det \mathbf{H}_E(\omega_0, \mu, \gamma) &= e^{-\pi\gamma/4} \\ &= 1 - \frac{\pi\gamma}{4} + \frac{\pi^2\gamma^2}{32} - \frac{\pi^3\gamma^3}{384} + \frac{\pi^4\gamma^4}{6144} - \frac{\pi^5\gamma^5}{122880} + \frac{\pi^6\gamma^6}{2949120} \\ &\quad - \frac{\pi^7\gamma^7}{82575360} + \frac{\pi^8\gamma^8}{2642411520} - \frac{\pi^9\gamma^9}{95126814720} \\ &\quad + \frac{\pi^{10}\gamma^{10}}{3805072588800} + \cdots, \end{aligned} \tag{53}$$

where the determinant has been expanded in terms of a Taylor series. Using (50), an analytical expression for the determinant of **H**, as

provided by the point mapping method, is given by

$$\det \mathbf{H}(\omega_0, \mu, \gamma) = 1 - \frac{\pi\gamma}{4} + \frac{\pi^2\gamma^2}{32} - \frac{\pi^2\gamma^3}{384} + \frac{\pi^4\gamma^4}{6144} - \frac{\pi^5\gamma^5}{122880} + \frac{\pi^6\gamma^6}{2949120} - \frac{\pi^7\gamma^7}{82575377} + \frac{\pi^8\gamma^8}{2642412963} - \frac{\pi^9\gamma^9}{95126930636} + \frac{\pi^{10}\gamma^{10}}{3805081784862} + \cdots \tag{54}$$

Note that det **H** given by (54) obtained from point mapping analysis is independent of the parameters ω_0 and μ as expected. This expression is in excellent agreement with the exact form (53) even for higher order coefficients. The coefficients of the point mapping expression in (54) differ from those of the exact result in (53) in the eleventh decimal place. By reducing the time step h used in generating the matrix **H** via (45), the accuracy of the point mapping results increases approaching the exact analytical expression.

Comparison with other methods of analysis: In order to compare our results with the perturbation and numerical solutions, define the characteristic exponents α_j of the linear system defined by

$$\alpha_j = \frac{1}{T}(\log|\lambda_j| + i\arg\lambda_j), \quad j = 1, 2, \ldots, N, \tag{55}$$

where λ_i are the eigenvalues of the matrix **H**. For two-dimensional systems, it is possible to obtain a closed-form expression for λ_i. When expanded in terms of the parameters ω_0, μ and γ, it is found that the characteristic multipliers λ_1 and λ_2 of the system in (47) have the following leading terms:

$$\lambda_1 = 1 - \left(\frac{\pi^3\gamma}{316} + \frac{\pi^4\gamma^2}{1263}\right)\mu^4 - \left(2\pi^2 + \frac{5\pi^3\gamma}{12} + \frac{\pi^4\gamma^2}{48} + \frac{\pi^5\gamma\mu^4}{59}\right)\omega_0^2 + \left(\frac{2\pi^4}{3} - \frac{191\pi^5\gamma}{180} - \frac{17\pi^6\gamma^2}{83} - \frac{2\pi^7\gamma^3}{125}\right)\omega_0^4 - \left(\frac{4\pi^6}{45} + \frac{892\pi^7\gamma}{159} + \frac{193\pi^8\gamma^2}{108} + \frac{85\pi^9\gamma^3}{328}\right)\omega_0^6 + \left(\frac{\pi^8}{158} - \frac{4043\pi^9\gamma}{120} - \frac{2016\pi^{10}\gamma^2}{131}\right)\omega_0^8 - \left(\frac{\pi^{10}}{3544} + \frac{12301\pi^{11}\gamma}{55}\right)\omega_0^{10} + \cdots$$

$$\lambda_2 = 1 - \frac{\pi\gamma}{4} + \frac{\pi^2\gamma^2}{32} - \frac{\pi^3\gamma^3}{384} + \frac{\pi^4\gamma^4}{6144} + \frac{\pi^3\gamma\mu^4}{316}$$
$$- \left(2\pi^2 - \frac{11\pi^3\gamma}{12} + \frac{\pi^4\gamma^2}{48} - \frac{\pi^5\gamma^3}{372} + \frac{\pi^6\gamma^4}{6583} - \frac{\pi^5\gamma\mu^4}{59}\right)\omega_0^2$$
$$+ \left(\frac{2\pi^4}{3} + \frac{161\pi^5\gamma}{180} + \frac{5\pi^6\gamma^2}{23} + \frac{\pi^7\gamma^3}{65}\right)\omega_0^4$$
$$- \left(\frac{4\pi^6}{45} - \frac{383\pi^7\gamma}{68} - \frac{491\pi^8\gamma^2}{275} - \frac{7\pi^9\gamma^3}{27}\right)\omega_0^6$$
$$+ \left(\frac{\pi^8}{158} + \frac{2392\pi^9\gamma}{71} + \frac{1739\pi^{10}\gamma^2}{113}\right)\omega_0^8$$
$$- \left(\frac{\pi^{10}}{3544} - \frac{12301\pi^{11}\gamma}{55}\right)\omega_0^{10} + \cdots \tag{56}$$

By fixing the parameters $\omega_0 = 1.06$ and $\gamma = 5$, the matrix $\mathbf{H}$ evaluated using (45) has the following functional form in terms of the parameter μ:

$$\mathbf{H}(\mu) = \begin{bmatrix} \frac{37}{258} + \frac{37\mu^2}{274} + \frac{3\mu^4}{40} + \frac{\mu^6}{71} + \frac{\mu^8}{213} - \frac{\mu^{10}}{3878} + \cdots, & \frac{1}{89} + \frac{\mu^4}{36} + \frac{\mu^8}{323} + \cdots \\ -\frac{1}{79} - \frac{7\mu^2}{83} + \frac{7\mu^4}{130} - \frac{\mu^6}{113} + \frac{\mu^8}{159} + \frac{\mu^{10}}{6205} + \cdots, & \frac{3}{22} - \frac{37\mu^2}{274} + \frac{11\mu^4}{191} - \frac{\mu^6}{71} + \frac{\mu^8}{362} + \frac{\mu^{10}}{3878} + \cdots \end{bmatrix} \tag{57}$$

Table I compares the characteristic exponents computed from numerical integration, perturbation analysis, and point mapping approach (using (57)) for various values of μ. The point mapping expressions for the 4th and 10th order mappings (respectively denoted by $\mathbf{H}_4$ and $\mathbf{H}_{10}$) were used to calculate the eigenvalues of $\mathbf{H}$. The third-order perturbation results were taken from Crespo da Silva and Hodges [6] where μ is treated as a small parameter. The direct integration result, considered here to represent the "exact result", was obtained by using a Runge–Kutta integrator to numerically compute the matrix $\mathbf{H}$.

The point mapping given in (50) leads to an important qualitative observation that $\mathbf{H}$ does not possess a linear term in the advance ratio μ, in fact $\mathbf{H}$ is of $\mathcal{O}(\mu^2)$. Since $\operatorname{tr}\mathbf{H}$ in this case is of $\mathcal{O}(\mu^4)$ and $\det\mathbf{H} = 1$, hence the characteristic multipliers λ_i given by (56) are of $\mathcal{O}(\mu^4)$. The absence of the linear term in μ explains why perturbation results given

TABLE I Characteristic exponents as a function of μ for a teetering rotor with $\omega_0 = 1.06$ and $\gamma = 5$ by different analysis methods

μ	*Point mapping*	*Direct integration*	*Perturbation* [6]
0.0	$-0.3124998 \pm i0.0128888$ ($\mathbf{H}_4$) $-0.3124998 \pm i0.0128888$ ($\mathbf{H}_{10}$)	$-0.3125000 \pm i0.0128888$	$-0.3125000 \pm i0.0111719$
0.1	$-0.3124998 \pm i0.0127956$ ($\mathbf{H}_4$) $-0.3124998 \pm i0.0127955$ ($\mathbf{H}_{10}$)	$-0.3125000 \pm i0.0127956$	$-0.3125000 \pm i0.0110621$
0.2	$-0.3124998 \pm i0.0113056$ ($\mathbf{H}_4$) $-0.3124998 \pm i0.0113050$ ($\mathbf{H}_{10}$)	$-0.3125000 \pm i0.9886949$	$-0.3125000 \pm i1.0009260$
0.3	-0.3072546, -0.3177436 ($\mathbf{H}_4$) -0.3072243, -0.3177753 ($\mathbf{H}_{10}$)	-0.3072245, -0.3177755	-0.3039590, -0.3210410
0.4	-0.2914364, -0.3335483 ($\mathbf{H}_4$) -0.2913664, -0.3336332 ($\mathbf{H}_{10}$)	-0.2913666, -0.3336334	-0.2901350, -0.3348650
0.5	-0.2762755, -0.3486353 ($\mathbf{H}_4$) -0.2760500, -0.3489496 ($\mathbf{H}_{10}$)	-0.2760502, -0.3489498	-0.2750700, -0.3499310

in Table I are fairly accurate for $\mu < 1$. It is seen that the lower-order point mapping results compare remarkably well with the direct integration result even for higher values of advance ratio μ, the result from $\mathbf{H}_{10}$ being indistinguishable. This is in contrast to the perturbation results where the accuracy decreases for higher values of μ, especially for the case $\rho = 1$ discussed in Section 4.2 (see Table II).

The final test to validate the accuracy of the point mapping method is to perform a bifurcation analysis of the trivial solution $\mathbf{x} = 0$ in parameter space and to compare it with a known solution. The conditions for bifurcation of a P-1 solution $\mathbf{x} = 0$ are established using Eqs. (16)–(18). The result is a functional relationship between ω_0, μ and γ which is satisfied when a bifurcation to a particular solution occurs. The first few terms in various bifurcation relationships obtained using the point mapping approach are given below.

Bifurcation of P-1 $\rightarrow$ P-1 (Emergence of harmonic solution):

$$\begin{aligned}\det(\mathbf{I} - \mathbf{H}) = &\left(4\pi^2 - \frac{\pi^3\gamma}{2} + \frac{\pi^4\gamma^2}{24} - \frac{\pi^5\gamma^3}{384}\right)\omega_0^2 \\ &- \left(\frac{4\pi^4}{3} - \frac{\pi^5\gamma}{6} + \frac{\pi^6\gamma^2}{80}\right)\omega_0^4 \\ &+ \left(\frac{8\pi^6}{45} - \frac{\pi^7\gamma}{45}\right)\omega_0^6 - \frac{4\pi^8\omega_0^8}{315} + \cdots \\ &= 0. \end{aligned} \tag{58}$$

TABLE II Characteristic exponents as a function of μ for a gimballed rotor with $\omega_0 = 1.06$ and $\gamma = 5$ by different analysis methods

μ	*Point mapping*	*Direct integration*	*Perturbation* [6]
0.0	$-0.3124998 \pm i0.0128888$ ($\mathbf{H}_4$) $-0.3124998 \pm i0.0128888$ ($\mathbf{H}_{10}$)	$-0.3125000 \pm i0.0128888$	$-0.3125000 \pm i0.0111172$
0.1	$-0.3124998 \pm i0.0121335$ ($\mathbf{H}_4$) $-0.3124998 \pm i0.0121336$ ($\mathbf{H}_{10}$)	$-0.3125000 \pm i0.0121337$	$-0.3125000 \pm i0.0104770$
0.2	$-0.3125002 \pm i0.0074591$ ($\mathbf{H}_4$) $-0.3124998 \pm i0.0074639$ ($\mathbf{H}_{10}$)	$-0.3125000 \pm i0.0074639$	$-0.3125005 \pm i0.0062757$
0.3	-0.2979163, -0.3270855 ($\mathbf{H}_4$) -0.2979058, -0.3270938 ($\mathbf{H}_{10}$)	-0.2979060, -0.3270940	-0.2997650, -0.3252350
0.4	-0.2837426, -0.3412396 ($\mathbf{H}_4$) -0.2836370, -0.3413627 ($\mathbf{H}_{10}$)	-0.2836371, -0.3413628	-0.2875730, -0.3374270
0.5	-0.2676597, -0.3571667 ($\mathbf{H}_4$) -0.2672531, -0.3577466 ($\mathbf{H}_{10}$)	-0.2672532, -0.3577468	-0.2735770, -0.3514230

Bifurcation of P-1 $\rightarrow$ P-2 (Emergence of subharmonic solution of order 2):

$$\begin{aligned}\det(\mathbf{I}+\mathbf{H}) &= 4 - \frac{\pi\gamma}{2} + \frac{\pi^2\gamma^2}{16} - \frac{\pi^3\gamma^3}{192} + \frac{\pi^4\gamma^4}{3072} \\ &\quad - \left(4\pi^2 - \frac{\pi^3\gamma}{2} + \frac{\pi^4\gamma^2}{24} - \frac{\pi^5\gamma^3}{384}\right)\omega_0^2 \\ &\quad + \left(\frac{4\pi^4}{3} - \frac{\pi^5\gamma}{6} + \frac{\pi^6\gamma^2}{80}\right)\omega_0^4 \\ &\quad - \left(\frac{8\pi^6}{45} - \frac{\pi^7\gamma}{45}\right)\omega_0^6 + \frac{4\pi^8\omega_0^8}{315} + \cdots \\ &= 0. \end{aligned} \tag{59}$$

Bifurcation of P-1 $\rightarrow$ P-3 (Emergence of subharmonic solution of order 3):

$$\begin{aligned}\det(\mathbf{I}+\mathbf{H}+\mathbf{H}^2) &= 9 - \frac{9\pi\gamma}{4} + \frac{15\pi^2\gamma^2}{32} - \frac{9\pi^3\gamma^3}{128} + \frac{2\pi^4\gamma^4}{241} \\ &\quad - \left(24\pi^2 - 6\pi^3\gamma + \pi^4\gamma^2 - \frac{\pi^5\gamma^3}{8}\right)\omega_0^2 \\ &\quad + \left(24\pi^4 - 6\pi^5\gamma + \frac{109\pi^6\gamma^2}{120}\right)\omega_0^4 \\ &\quad - \left(\frac{176\pi^6}{15} - \frac{44\pi^7\gamma}{15}\right)\omega_0^6 + \frac{344\pi^8\omega_0^8}{105} + \cdots \\ &= 0. \end{aligned} \tag{60}$$

Bifurcation of P-1 $\rightarrow$ P-4 (Emergence of subharmonic solution of order 4):

$$\begin{aligned}\det(\mathbf{I}+\mathbf{H}^2) = 4 &- \pi\gamma + \frac{\pi^2\gamma^2}{4} - \frac{\pi^3\gamma^3}{24} + \frac{\pi^4\gamma^4}{192} \\ &- \left(16\pi^2 - 4\pi^3\gamma + \frac{2\pi^4\gamma^2}{3} - \frac{\pi^5\gamma^3}{12}\right)\omega_0^2 \\ &+ \left(\frac{64\pi^4}{3} - \frac{16\pi^5\gamma}{3} + \frac{4\pi^6\gamma^2}{5}\right)\omega_0^4 \\ &- \left(\frac{512\pi^6}{45} - \frac{128\pi^7\gamma}{45}\right)\omega_0^6 + \frac{1024\pi^8\omega_0^8}{315} + \cdots \\ &= 0. \end{aligned} \tag{61}$$

Equations (58)–(61) define the region of the parameter space (ω_0, μ, γ) in which a bifurcation of the trivial solution $\mathbf{x}=0$ of (47) may occur. Note that a bifurcation of P-1 to P-3 for a two-dimensional system is possible only when $\gamma=0$ (see [17]).

Assume now that γ is fixed. Substituting a given value of ω_0 in one of the Eqs. (58)–(61), a polynomial equation in μ results. Solving this equation results in the value of μ at which various bifurcations may occur. Figure 1(a) shows the bifurcation curves in the (μ, ω_0) parameter plane obtained from point mapping of order $P=50$ for $\gamma=5$. For the range of parameters chosen, bifurcation from a P-1 solution to a P-2 solution does not exist and the curves shown in the figure indicate a P-1 to P-1 bifurcation. A detailed analysis of (60) and (61), with an increase in the order of truncation, reveals that they do not possess a non-trivial solution in the (μ, ω_0) plane. Thus, bifurcations of $\mathbf{x}=0$ to a P-1 or a P-2 solution are the only one possible (consistent with known analytical results for $\gamma>0$ (see [17])).

Since an analytical solution to bifurcation analysis of (47) is not available, results are compared with direct numerical integration of (47), which is considered here to be an "exact solution". In order to obtain bifurcation curves by direct integration, matrix $\mathbf{H}$ is computed on a very fine grid of points in the (μ, ω_0) parameter plane. The quantity on the left hand side of Eqs. (58)–(61) are satisfied to within a prescribed numerical precision. The result of direct integration is shown in Fig. 1(b). As can be seen, these two results

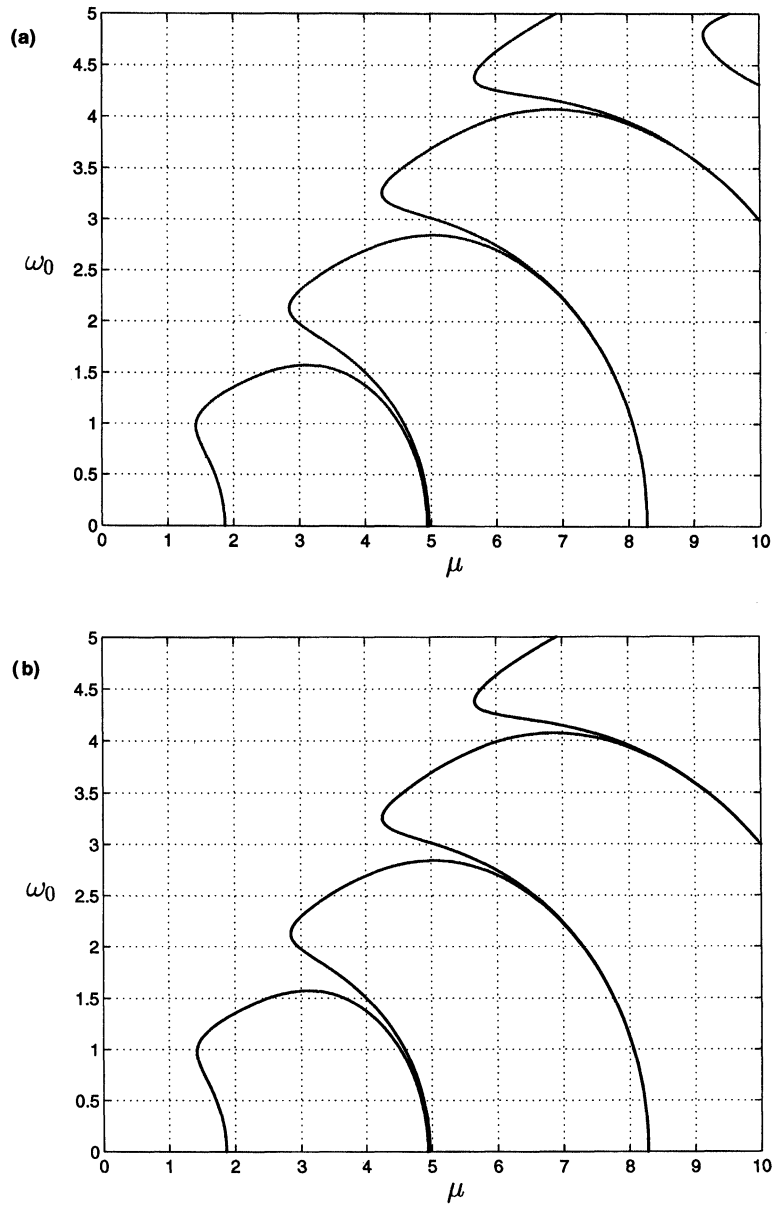

FIGURE 1 Bifurcation of the trivial P-1 solution to P-1 solution in the (μ, ω_0) parameter plane for a teetering rotor ($\rho = 0$): (a) Obtained by point mapping of order $P = 60$. (b) Obtained by direct integration.

are virtually identical. Point mapping results differs from the numerical solution only at the upper right-hand corner where $\omega_0 \approx 4.5$ and $\mu \approx 9.5$; improved accuracy can be obtained by increasing the point mapping order. It should be noted that even for *large values* of ω_0 and μ, the truncated point mapping solutions are very accurate when compared with "exact results" of direct integration.

4.2. Gimballed Rotor ($\rho = 1$)

The analytical expressions for the leading terms of components H_{ij} of the matrix $\mathbf{H}$, evaluated via Eq. (45), are presented below:

$$
\begin{aligned}
H_{11} &= 1 + \frac{\pi^3\gamma^2\mu}{237} - \frac{15\pi^2\gamma\mu^2}{377} - \left(2\pi^2 - \frac{\pi^3\gamma}{6} + \frac{\pi^4\gamma^2}{96}\right)\omega_0^2 \\
&\quad + \left(\frac{2\pi^4}{3} - \frac{\pi^5\gamma}{15}\right)\omega_0^4 - \frac{4\pi^6\omega_0^6}{45} + \cdots \\
H_{12} &= 2\pi - \frac{\pi^2\gamma}{4} + \frac{\pi^3\gamma^2}{48} - \frac{\pi^4\gamma^3}{768} \\
&\quad - \left\{\left(\frac{40\pi^2}{377} - \frac{46\pi^3}{681}\right)\gamma - \left(\frac{5\pi^3}{377} - \frac{2\pi^4}{237}\right)\gamma^2\right\}\mu \\
&\quad - \left\{\frac{4\pi^3}{3} - \frac{\pi^4\gamma}{6} + \frac{\pi^5\gamma^2}{80} - \left(\frac{17\pi^4}{613} - \frac{3\pi^5}{170}\right)\gamma\mu\right\}\omega_0^2 \\
&\quad + \left(\frac{4\pi^5}{15} - \frac{\pi^6\gamma}{30}\right)\omega_0^4 - \frac{8\pi^7\omega_0^6}{315} + \cdots \\
H_{21} &= \left\{-2\pi + \frac{\pi^2\gamma}{4} - \frac{\pi^3\gamma^2}{48} - \left(\frac{40\pi^2}{377} - \frac{46\pi^3}{681}\right)\gamma\mu\right\}\omega_0^2 \\
&\quad + \left(\frac{4\pi^3}{3} - \frac{\pi^4\gamma}{6}\right)\omega_0^4 - \frac{4\pi^5\omega_0^6}{15} + \cdots \\
H_{22} &= 1 - \frac{\pi\gamma}{4} + \frac{\pi^2\gamma^2}{32} - \frac{\pi^3\gamma^3}{384} - \frac{\pi^3\gamma^2\mu}{237} + \frac{15\pi^2\gamma\mu^2}{377} \\
&\quad - \left(2\pi^2 - \frac{\pi^3\gamma}{3} + \frac{\pi^4\gamma^2}{32}\right)\omega_0^2 + \left(\frac{2\pi^4}{3} - \frac{\pi^5\gamma}{10}\right)\omega_0^4 - \frac{4\pi^6\omega_0^6}{45} + \cdots
\end{aligned}
\tag{62}
$$

As mentioned for the case $\rho = 0$, higher order terms of $\mathbf{H}$ in (62) have coefficients which are progressively smaller in magnitude. The exact analytical expression for $\det \mathbf{H}_E$ is given by (53). The

corresponding expression produced by the point mapping in (62) is identical.

As before, the characteristic multipliers λ_i of the system in (47) obtained from (62) are as follows:

$$\begin{aligned}
\lambda_1 &= 1 - \left\{2\pi^2 + \frac{5\pi^3\gamma}{12} + \frac{\pi^4\gamma^2}{48} + \left(\frac{2\pi^3}{89} - \frac{5\pi^4}{23} + \frac{11\pi^5}{159}\right)\gamma\mu^2\right\}\omega_0^2 \\
&\quad + \left(\frac{2\pi^4}{3} - \frac{191\pi^5\gamma}{180} - \frac{17\pi^6\gamma^2}{83}\right)\omega_0^4 \\
&\quad - \left(\frac{4\pi^6}{45} + \frac{892\pi^7\gamma}{159}\right)\omega_0^6 - \frac{2\pi^8\omega_0^8}{315} + \cdots \\
\lambda_2 &= 1 - \frac{\pi\gamma}{4} + \frac{\pi^2\gamma^2}{32} - \frac{\pi^3\gamma^3}{384} + \frac{\pi^4\gamma^4}{6144} \\
&\quad - \left\{2\pi^2 - \frac{11\pi^3\gamma}{12} + \frac{\pi^4\gamma^2}{48} - \frac{\pi^5\gamma^3}{372} - \left(\frac{2\pi^3}{89} - \frac{5\pi^4}{23} + \frac{11\pi^5}{159}\right)\gamma\mu^2\right\}\omega_0^2 \\
&\quad + \left(\frac{2\pi^4}{3} + \frac{161\pi^5\gamma}{180} + \frac{5\pi^6\gamma^2}{23}\right)\omega_0^4 \\
&\quad - \left(\frac{4\pi^6}{45} - \frac{383\pi^7\gamma}{68}\right)\omega_0^6 + \frac{\pi^8\omega_0^8}{158} + \cdots
\end{aligned} \tag{63}$$

Table II provides the characteristic exponents for various values of μ with $\omega_0 = 1.06$, and $\gamma = 5$. The matrix $\mathbf{H}(\mu)$ in this case takes the form

$$\mathbf{H}(\mu) = \begin{bmatrix}
\frac{37}{258} - \frac{\mu}{532} + \frac{49\mu^2}{342} - \frac{\mu^3}{140} + \frac{21\mu^4}{209} + \frac{\mu^5}{197} & \frac{1}{89} - \frac{\mu}{332} - \frac{7\mu^2}{116} - \frac{7\mu^3}{183} + \frac{8\mu^4}{223} + \frac{\mu^5}{255} \\
+\frac{\mu^6}{75} + \frac{\mu^7}{1036} + \frac{\mu^8}{152} + \frac{\mu^9}{2465} + \frac{\mu^{10}}{2049} + \cdots, & -\frac{\mu^6}{190} - \frac{\mu^7}{899} + \frac{\mu^8}{485} + \frac{\mu^9}{8417} + \frac{\mu^{10}}{3172} + \cdots \\
-\frac{1}{79} - \frac{\mu}{453} - \frac{4\mu^2}{89} - \frac{\mu^3}{63} + \frac{5\mu^4}{86} - \frac{6\mu^5}{193} & \frac{3}{22} + \frac{\mu}{532} - \frac{9\mu^2}{67} + \frac{\mu^3}{140} + \frac{11\mu^4}{183} - \frac{\mu^5}{197} \\
-\frac{\mu^6}{139} - \frac{\mu^7}{302} + \frac{\mu^8}{240} - \frac{\mu^9}{2147} + \frac{\mu^{10}}{1194} + \cdots, & -\frac{\mu^6}{107} - \frac{\mu^7}{1036} + \frac{\mu^8}{4188} - \frac{\mu^9}{2465} + \frac{\mu^{10}}{2716} + \cdots
\end{bmatrix}. \tag{64}$$

It can be seen that the point mapping results compare remarkably well with the direct integration result. Also, it is evident that the results of perturbation analysis deviate significantly even for small values of μ. The reason why perturbation method performs poorly

for increasing values of μ is quite clear from the point mapping expression (62) which contains terms of $\mathcal{O}(\mu)$ and characteristic multipliers in (63) which are of $\mathcal{O}(\mu^2)$.

The first few terms in various bifurcation relationships generated from Eqs. (16)–(18) are given below.

Bifurcation of P-1 → P-1:

$$\begin{aligned}\det(\mathbf{I}-\mathbf{H}) &= \left(4\pi^2 - \frac{\pi^3\gamma}{2} + \frac{\pi^4\gamma^2}{24}\right)\omega_0^2 \\ &\quad - \left(\frac{4\pi^4}{3} - \frac{\pi^5\gamma}{6}\right)\omega_0^4 + \frac{8\pi^6\omega_0^6}{45} + \cdots \\ &= 0. \end{aligned} \tag{65}$$

Bifurcation of P-1 → P-2:

$$\begin{aligned}\det(\mathbf{I}+\mathbf{H}) &= 4 - \frac{\pi\gamma}{2} + \frac{\pi^2\gamma^2}{16} - \frac{\pi^3\gamma^3}{192} - \left(4\pi^2 - \frac{\pi^3\gamma}{2} + \frac{\pi^4\gamma^2}{24}\right)\omega_0^2 \\ &\quad + \left(\frac{4\pi^4}{3} - \frac{\pi^5\gamma}{6}\right)\omega_0^4 - \frac{8\pi^6\omega_0^6}{45} + \cdots \\ &= 0. \end{aligned} \tag{66}$$

Bifurcation of P-1 → P-3:

$$\begin{aligned}\det(\mathbf{I}+\mathbf{H}+\mathbf{H}^2) &= 9 - \frac{9\pi\gamma}{4} + \frac{15\pi^2\gamma^2}{32} - \frac{9\pi^3\gamma^3}{128} \\ &\quad - (24\pi^2 - 6\pi^3\gamma + \pi^4\gamma^2)\omega_0^2 \\ &\quad + (24\pi^4 - 6\pi^5\gamma)\omega_0^4 - \frac{176\pi^6\omega_0^6}{15} + \cdots \\ &= 0. \end{aligned} \tag{67}$$

Bifurcation of P-1 → P-4:

$$\begin{aligned}\det(\mathbf{I}+\mathbf{H}^2) &= 4 - \pi\gamma + \frac{\pi^2\gamma^2}{4} - \frac{\pi^3\gamma^3}{24} - \left(16\pi^2 - 4\pi^3\gamma + \frac{2\pi^4\gamma^2}{3}\right)\omega_0^2 \\ &\quad + \left(\frac{64\pi^4}{3} - \frac{16\pi^5\gamma}{3}\right)\omega_0^4 - \frac{512\pi^6\omega_0^6}{45} + \cdots \\ &= 0. \end{aligned} \tag{68}$$

Figure 2(a) shows the bifurcation curves in the (μ, ω_0) parameter plane obtained from point mapping of order $P=50$ for $\gamma=5$. As before, a detailed analysis of equations $\det(\mathbf{I}+\mathbf{H}^2)=0$ and

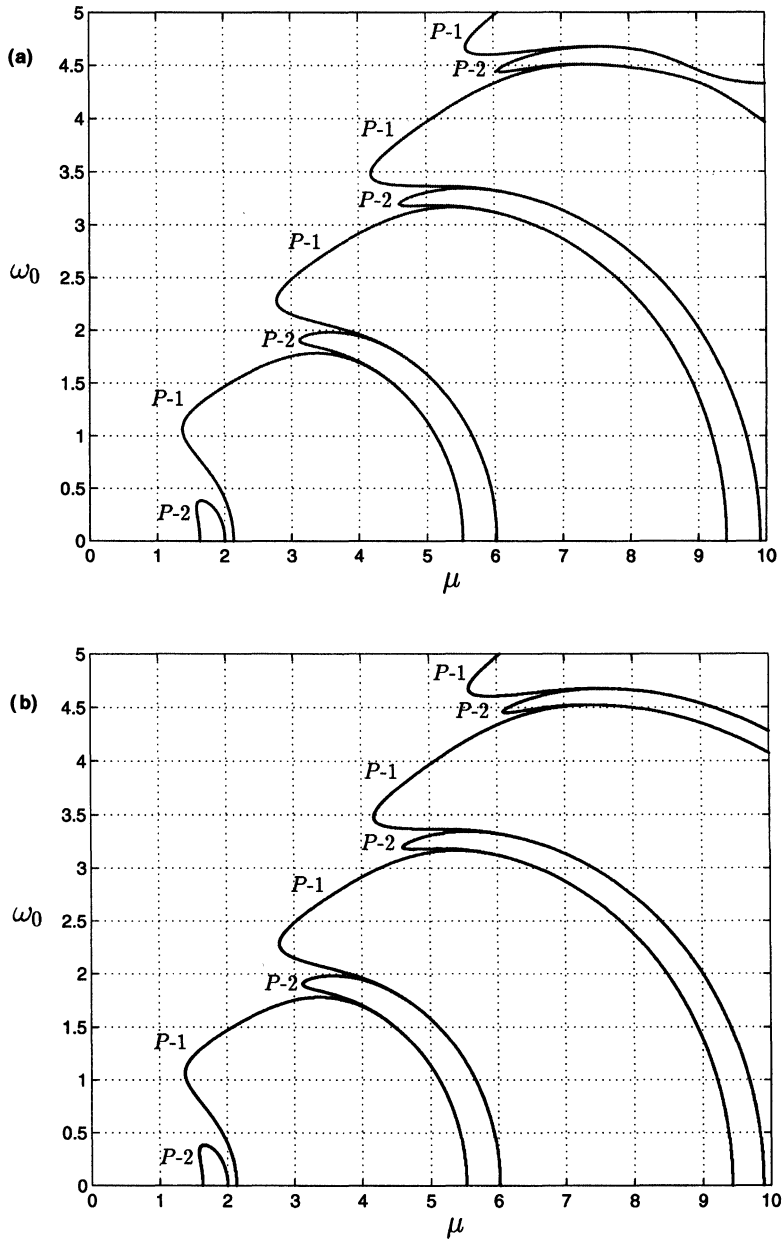

FIGURE 2 Bifurcation of the trivial P-1 solution to P-1 and P-2 solutions in the (μ, ω_0) parameter plane for a gimballed rotor ($\rho = 1$): (a) Obtained by point mapping of order $P = 60$. (b) Obtained by direct integration.

$\det(\mathbf{I}+\mathbf{H}+\mathbf{H}^2)=0$, with an increase in the order of truncation, reveals that they do not possess a non-trivial solution in the (μ, ω_0) plane. Thus, bifurcations of $\mathbf{x}=0$ to a P-1 or a P-2 solution are the only one possible. The agreement between the point mapping results shown in Fig. 2(a) and direct integration results shown in Fig. 2(b) is excellent. Closer agreement of point mapping results in the region $\omega_0 \approx 4.5$ and $\mu \approx 9$ with integration can be obtained by increasing the order P of the point mapping. As expected, for large range of parameter values, a higher order point mapping is required.

In summary, combining the results given by point mapping analysis for the rotor flapping motion, we observe that a bifurcation

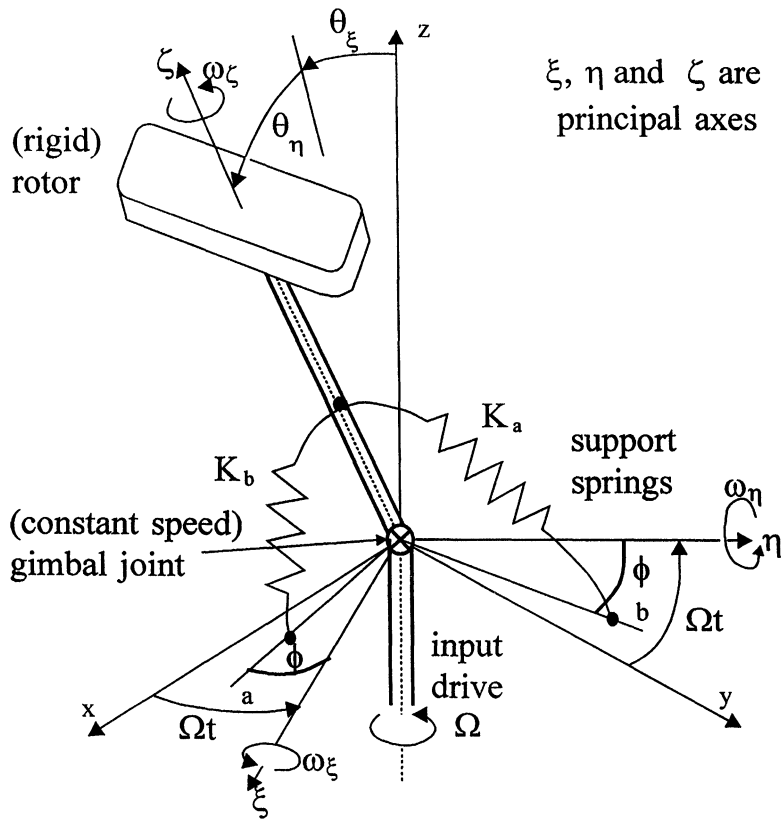

FIGURE 3 An unsymmetrical rigid rotor attached to an input shaft rotating at a constant speed Ω.

of the trivial solution $\mathbf{x}=0$ takes place when $\mu > 1.6355$. The flapping dynamics model under consideration is valid for only $0 < \mu < 0.3$, since for $\mu > 0$ reversed flow effects that are not included in the model become significant. However, we include here results for higher values of μ in order to demonstrate the accuracy of the Poincaré mapping approach when the design parameter is not small. Since, the model is valid for $0 < \mu < 0.3$, one concludes that for both cases of $\rho = 0$ and $\rho = 1$, bifurcation of the trivial solution may not occur in applications. It should be noted that when the coupled flap-lag-torsion motion of a rotor (described by a higher order linear periodic differential equation) is analyzed, bifurcation may occur for much lower values of μ (see Peters [24]).

5. GROUND RESONANCE OF A ROTORCRAFT

Analysis of a simple model of ground resonance of a helicopter (see Fig. 3 taken from [3]) is performed here to demonstrate the capability of the point mapping method to study multi degrees-of-freedom systems. The system consists of a rigid rotor with elastic restraints whose input shaft rotates at a constant speed Ω. We consider the case of external stiffness for which $\phi = \Omega t$. The equation of motion of the rigid rotor for small angular displacements θ_ξ and θ_η may be expressed as

$$\frac{d\mathbf{x}}{d\tau} = \mathbf{A}(\tau)\mathbf{x}, \tag{69}$$

$$\mathbf{A}(\tau) = \begin{bmatrix} 0 & 0 & 1 & 0 \\ 0 & 0 & 0 & 1 \\ -\dfrac{2\alpha-(1-\epsilon_i)+\frac{1}{r^2}(1+\epsilon_s\cos 2\tau)}{1+\epsilon_i} & -\dfrac{\epsilon_s \sin 2\tau}{r^2(1+\epsilon_i)} & 0 & \dfrac{2(1-\alpha)}{1+\epsilon_i} \\ \dfrac{\epsilon_s \sin 2\tau}{r^2(1-\epsilon_i)} & -\dfrac{2\alpha-(1+\epsilon_i)+\frac{1}{r^2}(1-\epsilon_s\cos 2\tau)}{1-\epsilon_i} & -\dfrac{2(1-\alpha)}{1-\epsilon_i} & 0 \end{bmatrix},$$

where $\mathbf{x} = [\theta_\xi, \theta_\eta, \dot{\theta}_\xi, \dot{\theta}_\eta]^T$ is the state vector. The inertia anisotropy ϵ_i, stiffness anisotropy ϵ_s, and axial inertia ratio α are defined as

$$\begin{aligned} \epsilon_i &= \frac{I_\xi - I_\eta}{I_\xi + I_\eta}, \quad -1 < \epsilon_i \leq 1, \\ \epsilon_s &= \frac{k_a - k_b}{k_a + k_b}, \quad 0 \leq \epsilon_s \leq 1, \\ \alpha &= \frac{I_\zeta}{I_\xi + I_\eta}, \quad |\epsilon_i| < \alpha < 1, \end{aligned} \tag{70}$$

and the frequency ratio is given by

$$r = \frac{\omega_0}{\Omega}, \quad \omega_0 = \sqrt{\frac{k_a + k_b}{I_\xi + I_\eta}}. \tag{71}$$

Systems of the type (69) also find applications in high-speed rotating machinery, see [3,5,7,14]. The two anisotropy parameters, ϵ_i and ϵ_s, play a significant role in characterizing system's stability at higher rotational speeds.

Consider the problem of finding stability boundary curves in four-dimensional space of parameters r, α, ϵ_i, and ϵ_s. To evaluate the matrix $\mathbf{H}(r, \alpha, \epsilon_i, \epsilon_s)$ associated with the system in (69), set $t_0 = 0$, $T = \pi$, $N_t = 100$, $P = 4$. Truncation is carried out to keep homogeneous terms of the type

$$\frac{\alpha^{k_2} \epsilon_i^{k_3} \epsilon_k^{k_4}}{r^{2k_1}}, \quad k_1 + k_2 + k_3 + k_4 \leq P.$$

The resulting analytical expression for the matrix $\mathbf{H}(r, \alpha, \epsilon_i, \epsilon_s)$ reveals symmetry among its components. The symmetry is with respect to the parameters ϵ_i and ϵ_s which implies that the matrix $\mathbf{H}$ has only eight independent elements. The remaining eight elements are either odd or even functions. In terms of the components H_{ij}, the matrix $\mathbf{H}$ can be expressed as

$$\mathbf{H}(r, \alpha, \epsilon_i, \epsilon_s) = \begin{bmatrix} H_{11}(r, \alpha, \epsilon_i, \epsilon_s) & H_{12}(r, \alpha, \epsilon_i, \epsilon_s) & H_{13}(r, \alpha, \epsilon_i, \epsilon_s) & H_{14}(r, \alpha, \epsilon_i, \epsilon_s) \\ -H_{12}(r, \alpha, -\epsilon_i, -\epsilon_s) & H_{11}(r, \alpha, -\epsilon_i, -\epsilon_s) & -H_{14}(r, \alpha, -\epsilon_i, -\epsilon_s) & H_{13}(r, \alpha, -\epsilon_i, -\epsilon_s) \\ H_{31}(r, \alpha, \epsilon_i, \epsilon_s) & H_{32}(r, \alpha, \epsilon_i, \epsilon_s) & H_{33}(r, \alpha, \epsilon_i, \epsilon_s) & H_{34}(r, \alpha, \epsilon_i, \epsilon_s) \\ -H_{32}(r, \alpha, -\epsilon_i, -\epsilon_s) & H_{31}(r, \alpha, -\epsilon_i, -\epsilon_s) & -H_{34}(r, \alpha, -\epsilon_i, -\epsilon_s) & H_{33}(r, \alpha, -\epsilon_i, -\epsilon_s) \end{bmatrix} \tag{72}$$

In order to verify the above symmetry, an exhaustive numerical study has been carried out. The matrix **H** was computed by direct integration in the four-dimensional parameter space $(r, \alpha, \epsilon_i, \epsilon_s)$ by forming a large, uniformly spaced grid. This study asserted that the matrix **H** possesses the symmetry indicated by (72). Thus, the point mapping approach presented here has the unique feature of unraveling hidden symmetry in the dynamics of the model. The leading terms of the independent elements of the matrix **H** are given below:

$$
\begin{aligned}
H_{11}(r,\alpha,\epsilon_i,\epsilon_s) &= -1+\pi^2\alpha\left(1-\epsilon_i+2\epsilon_i^2-\frac{\pi^2\alpha^2}{3}\right)\\
&\quad+\frac{\pi^2}{r^2}\left\{\frac{1}{2}\left(1+\epsilon_s+\epsilon_i^2-\epsilon_i\epsilon_s\right)-\pi\alpha\left(\frac{\pi}{6}+\frac{\pi\alpha}{6}-\frac{962\epsilon_i}{1409}\right)\right\}\\
&\quad-\frac{\pi^4}{r^4}\left\{\frac{1}{24}-\frac{\pi^2\alpha}{120}+\frac{\epsilon_s}{12}\right\}+\frac{\pi^6}{720r^6}+\cdots\\
H_{12}(r,\alpha,\epsilon_i,\epsilon_s) &= \pi\left(1+\epsilon_i+\epsilon_i^2+\epsilon_i^3\right)\\
&\quad+\pi\alpha\left(2\epsilon_i+3\epsilon_i^2-\frac{2\pi^2\alpha}{3}-\frac{155\pi^2\alpha\epsilon_i}{593}\right)\\
&\quad-\frac{\pi^2}{r^2}\left\{\frac{\pi}{6}+\frac{122\pi\epsilon_i}{1867}+\frac{\pi\epsilon_s}{6}+\frac{158\pi\epsilon_i^2}{681}+\frac{\pi\epsilon_i\epsilon_s}{6}\right.\\
&\qquad\left.+\pi\alpha\left(\frac{1}{3}+\frac{52\pi\epsilon_i}{625}-\frac{\epsilon_s}{3}-\frac{\pi^2\alpha}{10}\right)\right\}\\
&\quad+\frac{\pi^4}{r^4}\left\{\frac{\pi}{120}+\frac{\pi\alpha}{30}+\frac{\pi\epsilon_i}{584}+\frac{\pi\epsilon_s}{60}\right\}-\frac{\pi^7}{5040r^6}+\cdots\\
H_{13}(r,\alpha,\epsilon_i,\epsilon_s) &= -\pi\left(1+\epsilon_i+\epsilon_i^2+\epsilon_i^3\right)\\
&\quad-\pi\alpha\left(2\epsilon_i+3\epsilon_i^2-\frac{2\pi^2\alpha}{3}-\frac{155\pi^2\alpha\epsilon_i}{593}\right)\\
&\quad+\frac{\pi^2}{r^2}\left\{\frac{\pi}{6}+\frac{79\pi}{681}\left(\epsilon_i+2\epsilon_i^2+\epsilon_i\epsilon_s\right)+\frac{\pi\epsilon_s}{6}\right.\\
&\qquad\left.+\pi^2\alpha\left(\frac{2968\epsilon_i}{22557}-\frac{\pi\alpha}{10}\right)\right\}\\
&\quad-\frac{\pi^4}{r^4}\left\{\frac{\pi}{120}+\frac{\pi\epsilon_i}{584}+\frac{\pi\epsilon_s}{60}\right\}+\frac{\pi^7}{5040r^6}+\cdots+\cdots\\
H_{14}(r,\alpha,\epsilon_i,\epsilon_s) &= \pi^2\alpha\left(1-\epsilon_i+2\epsilon_i^2-\frac{\pi^2\alpha^2}{3}\right)\\
&\quad-\frac{\pi^2}{r^2}\left\{\frac{\pi^2\alpha}{6}\left(1-\epsilon_i\right)+\frac{\epsilon_i\epsilon_s}{2}\right\}+\frac{\pi^6\alpha}{120r^6}+\cdots
\end{aligned}
$$

$$
\begin{aligned}
H_{31}(r,\alpha,\epsilon_i,\epsilon_s) &= -\pi\left(1-\epsilon_i+\epsilon_i^2-\epsilon_i^3\right)\\
&\quad+\pi\alpha\left(2-2\epsilon_i+3\epsilon_i^2+\frac{2\pi^2\alpha}{3}-\frac{2\pi^2\alpha\epsilon_i}{3}-\frac{4\pi^2\alpha^2}{3}\right)\\
&\quad+\frac{\pi^2}{r^2}\left\{\frac{257\pi}{959}-\frac{148\pi\epsilon_i}{681}+\frac{296\pi\epsilon_i^2}{681}+\frac{10\pi\epsilon_i\epsilon_s}{681}-\frac{122\pi\epsilon_s}{1867}\right.\\
&\qquad\left.-\pi\alpha\left(\frac{\pi}{3}-\frac{382\pi\epsilon_i}{1673}-\frac{\epsilon_s}{3}+\frac{95\pi^2\alpha}{567}\right)\right\}\\
&\quad-\frac{\pi^4}{r^4}\left\{\frac{20\pi}{793}-\frac{\pi\alpha}{60}-\frac{33\pi\epsilon_i}{1967}+\frac{11\pi\epsilon_s}{643}\right\}+\frac{\pi^7}{959r^6}+\cdots\\
H_{32}(r,\alpha,\epsilon_i,\epsilon_s) &= \pi^2\alpha\left(1+\epsilon_i+2\epsilon_i^2-2\alpha-\frac{\pi^2\alpha^2}{3}\right)\\
&\quad-\frac{\pi^2}{r^2}\left\{\epsilon_s+\frac{\epsilon_i\epsilon_s}{2}+\alpha\left(\frac{257\pi^2}{959}+\frac{\pi^2\epsilon_i}{6}-\epsilon_s-\frac{\pi^2\alpha}{3}\right)\right\}\\
&\quad+\frac{\pi^4}{r^4}\left\{\frac{20\pi^2\alpha}{793}+\frac{\epsilon_s}{6}\right\}+\cdots\\
H_{33}(r,\alpha,\epsilon_i,\epsilon_s) &= -1-\pi^2\alpha\left(1+\epsilon_i+2\epsilon_i^2-2\alpha-\frac{\pi^2\alpha^2}{3}\right)\\
&\quad+\frac{\pi^2}{r^2}\left\{\frac{1}{2}(1+\epsilon_s+\epsilon_i^2+\epsilon_i\epsilon_s)+\pi\alpha\left(\frac{\pi}{6}-\frac{\pi\alpha}{2}+\frac{962\epsilon_i}{1409}\right)\right\}\\
&\quad-\frac{\pi^4}{r^4}\left\{\frac{1}{24}+\frac{\pi^2\alpha}{120}+\frac{\epsilon_s}{12}\right\}+\frac{\pi^6}{720r^6}+\cdots\\
H_{34}(r,\alpha,\epsilon_i,\epsilon_s) &= -\pi\left(1-\epsilon_i+\epsilon_i^2-\epsilon_i^3\right)\\
&\quad+\pi\alpha\left(2-2\epsilon_i+3\epsilon_i^2+\frac{2\pi^2\alpha}{3}-\frac{2\pi^2\alpha\epsilon_i}{3}-\frac{4\pi^2\alpha^2}{3}\right)\\
&\quad+\frac{\pi^2}{r^2}\left\{\frac{\pi}{6}(1-\epsilon_i+2\epsilon_i^2-\epsilon_s)\right.\\
&\qquad\left.+\frac{122\pi\epsilon_i\epsilon_s}{1867}-\frac{2\pi\alpha}{3}\left(1-\epsilon_i+\frac{3\pi^2\alpha^2}{20}\right)\right\}\\
&\quad-\frac{\pi^4}{r^4}\left\{\frac{\pi}{120}-\frac{\pi\alpha}{20}-\frac{\pi\epsilon_i}{120}-\frac{\pi\epsilon_s}{60}\right\}+\frac{\pi^7}{5040r^6}+\cdots
\end{aligned}
\tag{73}
$$

Since $\operatorname{tr}\mathbf{A}=0$, the dynamical system given in (69) preserves volume in state space and $\det\mathbf{H}=1$. To check the accuracy of $\mathbf{H}$

given above, the determinant of **H** was evaluated from (73) to yield

$$\begin{aligned}\det \mathbf{H} = {} & 1 + 1.6 \times 10^{-8}\alpha - 8.0 \times 10^{-8}\alpha^2 + 2.1 \times 10^{-7}\alpha^3 \\ & + (1.6 \times 10^{-8}\alpha - 1.4 \times 10^{-7}\alpha^2)\epsilon_i^2 \\ & - \frac{1}{r^2}\{4.0 \times 10^{-8} - 1.6 \times 10^{-7}\alpha + 3.2 \times 10^{-7}\alpha^2 \\ & \quad + (4.0 \times 10^{-8} - 2.9 \times 10^{-7}\alpha)\epsilon_i^2\} \\ & - \frac{1}{r^4}\{4.0 \times 10^{-8} - 8.0 \times 10^{-8}\alpha + 4.8 \times 10^{-8}\alpha^2 \\ & \quad + 8.8 \times 10^{-8}\epsilon_i^2 + 1.6 \times 10^{-8}\epsilon_s^2\} \\ & - 2.7 \times 10^{-9}\frac{1}{r^6} + \cdots \end{aligned} \tag{74}$$

The coefficients in the above expression decreases significantly with decreasing h and in the limit as $h \to 0$, $\det \mathbf{H} \to 1$.

Using Eqs. (16)–(18), the matrix **H** given in (73) yields the following analytical expressions for determining the bifurcation of the trivial P-1 solution $\mathbf{x} = 0$.

Bifurcation of P-1 $\to$ P-1:

$$\begin{aligned}\det(\mathbf{I} - \mathbf{H}) = {} & 16\left(1 - \pi^2\alpha^2 + \frac{\pi^4\alpha^4}{3} - 32\pi^2\alpha^2\epsilon_i^2\right) \\ & - \frac{8\pi^2}{r^2}\left\{1 - \frac{2\pi^2\alpha^2}{3} + (1+\alpha)\epsilon_i^2\right\} \\ & + \frac{\pi^4}{r^4}\left\{\frac{5}{3} - \frac{11\pi^2\alpha^2}{15} + \frac{2132\epsilon_i^2}{681} - \frac{\epsilon_s^2}{3}\right\} \\ & - \frac{17\pi^6}{90r^6} + \frac{13\pi^8}{1008r^8} + \cdots \\ = {} & 0. \end{aligned} \tag{75}$$

Bifurcation of P-1 $\to$ P-2:

$$\det(\mathbf{I} + \mathbf{H}) = \frac{\pi^4}{r^4}\left\{1 - \frac{\pi^2\alpha^2}{3} + 2\epsilon_i^2 - \epsilon_s^2\right\} - \frac{\pi^6}{6r^4} + \frac{\pi^8}{80r^8} + \cdots = 0. \tag{76}$$

Bifurcation of P-1 → P-3:

$$\det(\mathbf{I}+\mathbf{H}+\mathbf{H}^2) = 1 - 8\pi^2\alpha^2 + \frac{56\pi^4\alpha^4}{3} - 16\pi^2\alpha^2\epsilon_i^2 - \frac{4\pi^2}{r^2}\left\{1 - \frac{14\pi^2\alpha^2}{3} + (1+\alpha)\epsilon_i^2\right\} + \frac{\pi^4}{r^4}\left\{\frac{19}{3} - \frac{233\pi^2\alpha^2}{15} + \frac{4423\epsilon_i^2}{352} - \frac{5\epsilon_s^2}{3}\right\} - \frac{451\pi^6}{90r^6} + \frac{276\pi^8}{133r^8} + \cdots = 0. \tag{77}$$

Bifurcation of P-1 → P-4:

$$\det(\mathbf{I}+\mathbf{H}^2) = 16\left(1 - 4\pi^2\alpha^2 + \frac{16\pi^4\alpha^4}{3} - 8\pi^2\alpha^2\epsilon_i^2\right) - \frac{32\pi^2}{r^2}\left\{1 - \frac{8\pi^2\alpha^2}{3} + (1+\alpha)\epsilon_i^2\right\} + \frac{16\pi^4}{r^4}\left\{\frac{5}{3} - \frac{44\pi^2\alpha^2}{15} + \frac{63976\epsilon_i^2}{19489} - \frac{5\epsilon_s^2}{3}\right\} - \frac{544\pi^6}{45r^6} + \frac{208\pi^8}{63r^8} + \cdots = 0. \tag{78}$$

We fix the axial inertia ratio $\alpha = 0.5$, and consider two cases of importance below, $\epsilon_i = 0$, and $\epsilon_i = \epsilon_s$. The points r_0 where bifurcation branches may evolve on the r-axis ($\epsilon_s = 0$) are obtained by solving the bifurcation conditions (75)–(78) provided by the analytical point mapping. These points are identical for both the two cases. Table III shows the bifurcation points as computed by solving Eqs. (75)–(78) and compares them to those obtained by brute force numerical integration. For the purpose of this study, the results from numerical computations are considered to be the "exact" solution. It can be observed from Table III that the two results coincide except when r is very small; by increasing the order P of the point mapping, a closer agreement is readily obtained. The analytical point mapping results implies that bifurcation of the trivial solution $\mathbf{x} = 0$ (along the r-axis) to harmonic and subharmonics of order 2, 3, and 4 can no longer take place for frequency ratio $r > 1.5$. In addition, it also indicates that

TABLE III Bifurcation points r_0 on the frequency axis for both Cases I and II

P-1 *to P*-1 *Bifurcation*		*P*-1 *to P*-2 *Bifurcation*		*P*-1 *to P*-3 *Bifurcation*		*P*-1 *to P*-4 *Bifurcation*	
Exact	*PM*	*Exact*	*PM*	*Exact*	*PM*	*Exact*	*PM*
0.7071068	0.7071066	0.7071068	0.7071068	1.4999999	1.4999999	1.1547002	1.1547002
0.4082483	0.4082482	0.4082483	0.4082480	0.9486833	0.9486833	0.5164075	0.5164075
0.2886751	0.2886746	0.2886751	0.2886750	0.5669467	0.5669467	0.3380549	0.3380549
0.2236068	0.2236065	0.2236067	0.2236057	0.4743416	0.4743414	0.2519779	0.2519779
0.1825740	0.1825718	0.1825741	0.1825733	0.3585685	0.3585682	0.2010049	0.2010049
0.1543033	0.1543022	0.1543031	0.1543007	0.3198011	0.3198010	0.1672452	0.1672452
0.1336303	0.1336287	0.1336305	0.1336275	0.2631174	0.2631172	0.1432219	0.1432219
0.1178509	0.1178472	0.1178507	0.1178459	0.2417468	0.2417460	0.1252420	0.1252420
0.1054087	0.1054037	0.1054088	0.1054031	0.2080125	0.2080112	0.1112818	0.1112772
0.0953458	0.0953500	0.0953456	0.0953257	0.1944611	0.1944602	0.1001240	0.1001150
0.0870380	0.0870380	0.0870382	0.0870223	0.1720617	0.1720612	0.0910028	0.0910135
0.0800630	0.0800630	0.0800631	—	0.1626976	0.1626937	0.0834053	0.0819889
0.0741233	—	0.0741237	—	0.1467345	0.1467315	0.0769794	—

bifurcation points cluster around $r=0$. This feature may lead to the existence of many periodic solutions for small values of r.

Case I: $\epsilon_i=0$, $\alpha=0.5$: The condition $\epsilon=0$ leads to the symmetrical inertia case (that is, $I_\xi=I_\eta$). Figure 4 shows stability boundary curves in the (r,ϵ_s) plane as determined by point mapping of order $P=50$. The matrix $\mathbf{H}(r,\epsilon_s)$ was evaluated by fixing the above parameter values. To obtain accurate bifurcation branches, the matrix $\mathbf{H}(r,\epsilon_s)$ was directly employed to compute the various determinants involved in determining bifurcation points. Using the Newton–Raphson iteration, and starting with the location of bifurcation points given by Table III on the r-axis as initial guesses, bifurcation branches corresponding to P-1, P-2, P-3 and P-4 solutions were evaluated. For small values of the frequency ratio r (say $r<0.2$), the point mapping results indicate that bifurcation of the trivial solution $\mathbf{x}=0$ to harmonic and subharmonic solutions occurs for a many values of r. This indicates that the separation of stable and unstable regions in the (r,ϵ_s) plane becomes narrower

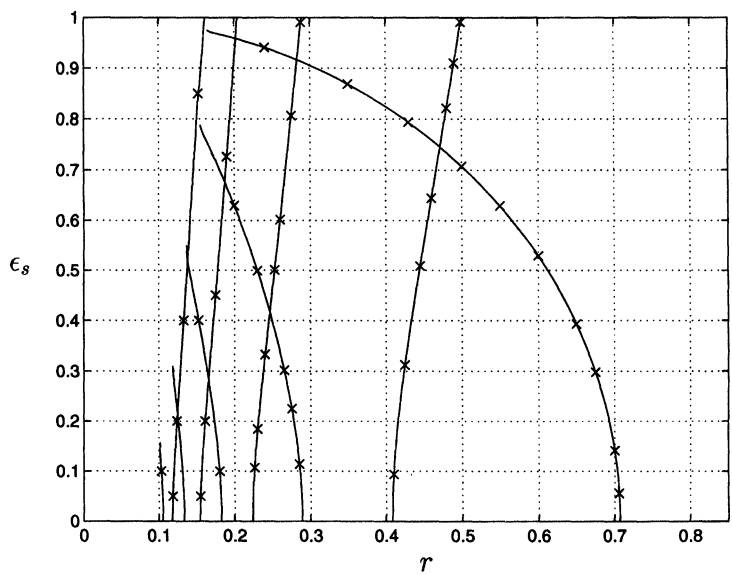

FIGURE 4(a)

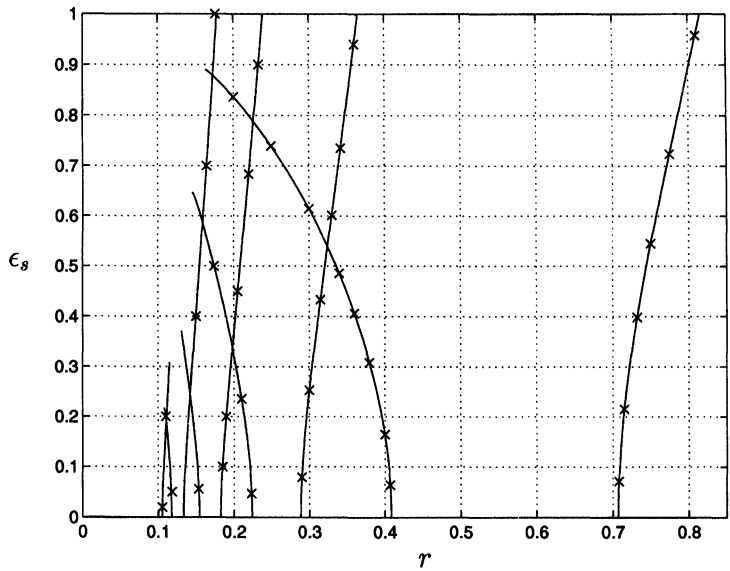

FIGURE 4(b)

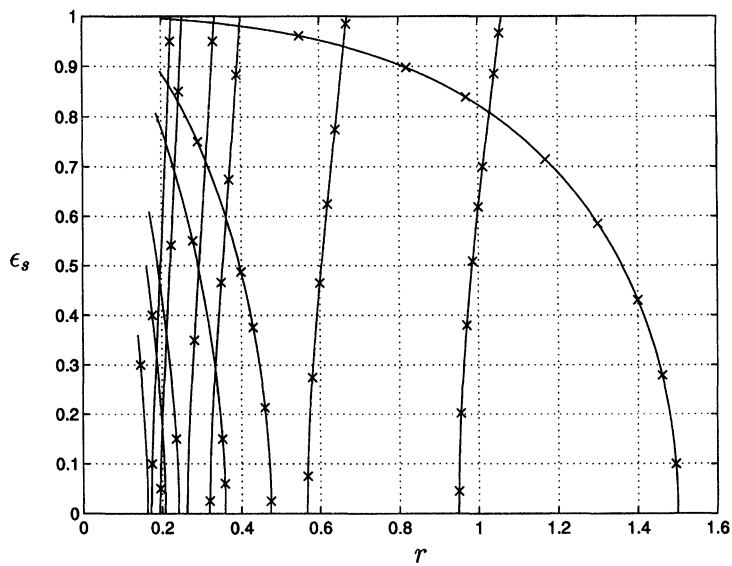

FIGURE 4(c)

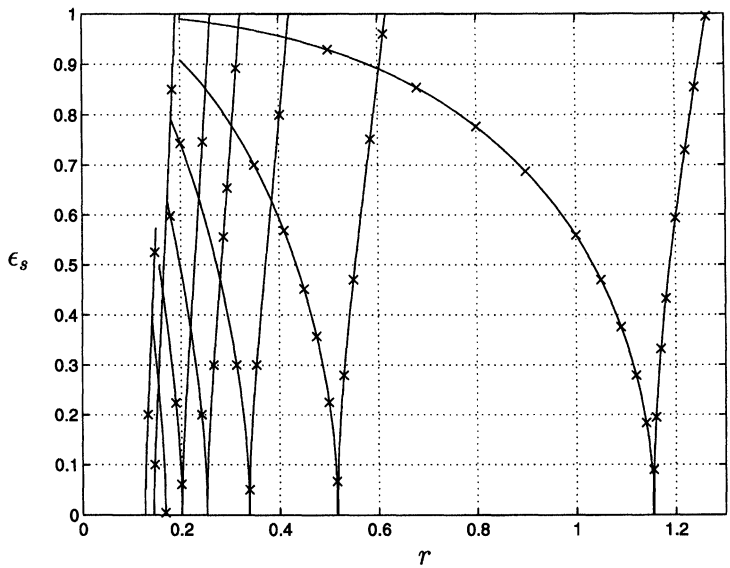

FIGURE 4(d)

FIGURE 4 Bifurcation of the trivial P-1 solution ($\mathbf{x}=0$) in the (r, ϵ_s) parameter plane for rotors with symmetrical inertia properties ($\epsilon_i=0$) obtained by point mapping of order $P=50$ for $\alpha=0.5$. Direct integration results are represented by " $\times$ ". (a) Bifurcation to P-1 solution. (b) Bifurcation to P-2 solution. (c) Bifurcation to P-3 solution. (d) Bifurcation to P-4 solution.

with decreasing values of r implying that avoidance of instability for these values of r is extremely difficult.

Case II: $\epsilon_i=\epsilon_s$, $\alpha=0.5$: For this case of equal inertia and stiffness anisotropy, the parameter ϵ_s has the range $0\leq\epsilon_s\leq 0.5$. By fixing $P=50$, the matrix $\mathbf{A}$ in (69) was expanded in series in terms of ϵ_i. The resulting $\mathbf{A}$ matrix was employed to evaluate the matrix $\mathbf{H}(r, \epsilon_s)$. Figure 5 shows the bifurcation of the trivial P-1 solution to P-1, P-2, P-3, and P-4 solutions in the (r, ϵ_s) plane. The effect of including inertia anisotropy ϵ_i is evident by comparing Fig. 5 with Fig. 4. Even though the bifurcation points along the r-axis for $\epsilon_s=0$ are the same as in Case I, the bifurcation curves differ substantially for $\epsilon_s>0$. Notice also the widening of the separation of the region between stable and unstable zones, resulting from including inertia anisotropy ϵ_i.

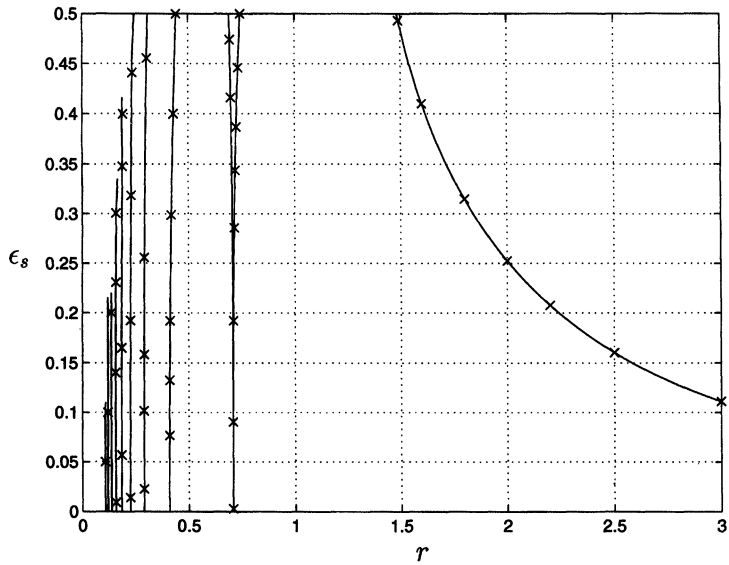

FIGURE 5(a)

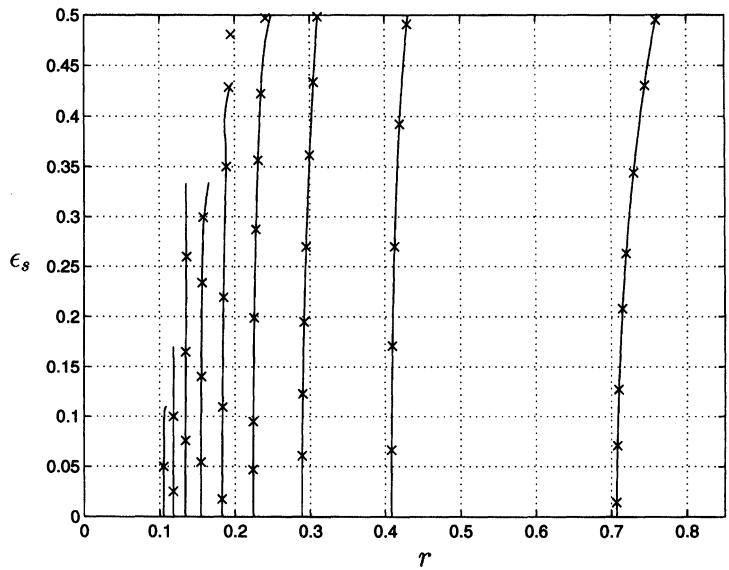

FIGURE 5(b)

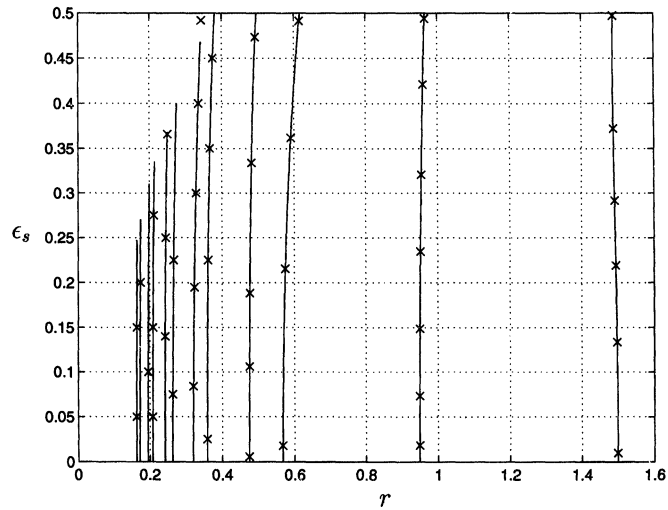

FIGURE 5(c)

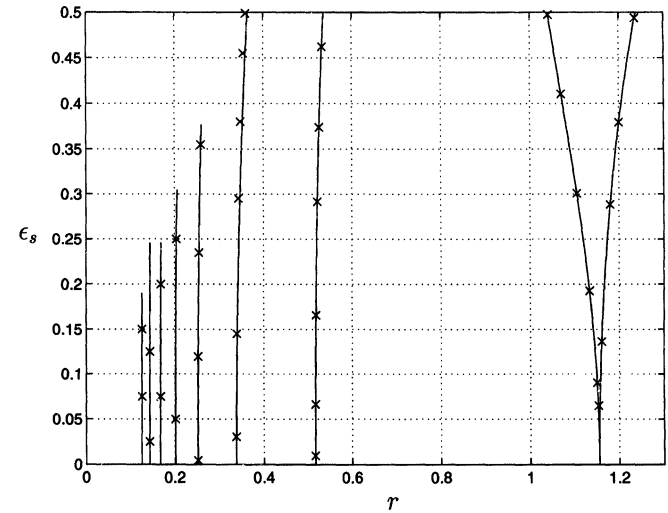

FIGURE 5(d)

FIGURE 5 Bifurcation of the trivial P-1 solution ($\mathbf{x}=0$) in the (r, ϵ_s) parameter plane for rotors with equal elastic and inertia properties ($\epsilon_i=\epsilon_s$) obtained by point mapping of order $P=50$ for $\alpha=0.5$. Direct integration results are represented by "$\times$". (a) Bifurcation to P-1 solution. (b) Bifurcation to P-2 solution. (c) Bifurcation to P-3 solution. (d) Bifurcation to P-4 solution.

The accuracy of the above calculations for bifurcation is assessed by comparing them with a direct numerical integration of (69) over one period of time using a fourth-order Runge–Kutta integration scheme. Newton–Raphson iteration is employed to solve the appropriate bifurcation condition (16)–(18). For initial guesses, the point mapping solution for bifurcation points displayed in Figs. 4 and 5 are used. Results obtained by direct integration of (69) are indicated in these figures by '×'. The proposed point mapping results show excellent agreement with the numerical solution, especially for $r > 0.2$. Since the equation of motion (69) contains $1/r^2$, bifurcation points are computationally difficult to obtain as $r \to 0$. This observation also naturally applies to the point mapping solution given in (69). However, as opposed to numerical integration, by evaluating a higher order point mapping, the proposed approach can be very effective in obtaining bifurcation branches close to $r = 0$.

Both cases discussed above for ground resonance problem indicate complex bifurcation patterns in the frequency domain. The point mapping results have not only revealed qualitative dynamics but it has also produced quantitative results in excellent agreement with exact results. The improvement and convergence of the point mapping analysis with increasing order of approximation, not further elaborated here, have been observed for the higher dimensional problem. Moreover, the validity of the point mapping approach for a large range of parameter values is established for the class of systems studied.

6. CONCLUSIONS

It is demonstrated in this paper that the point mapping method provides both analytical stability and bifurcation conditions for periodic systems encountered in engineering problems, e.g. rotorcraft dynamics. The traditional methods of analysis, classical perturbation and numerical procedures included, have been compared with the proposed point mapping approach. While perturbation procedures demand the presence of a small parameter, the point mapping method provides a solution without such requirements. The results presented here for problems in rotorcraft dynamics illustrate the

capability of the point mapping method to provide accurate analytical solution for multi-dimensional and multi-parameter systems. Also, the validity of analytical results to large variations in parameter values has been clearly demonstrated.

Acknowledgement

The research reported here was partially supported by the National Science Foundation grant CMS-9700467.

References

[1] Arnold, V.I., *Mathematical Methods of Classical Mechanics*, Springer-Verlag, New York, 1980.
[2] Bernussou, J., *Point Mapping Stability*, Pergamon, Oxford, 1977.
[3] Bielawa, R.L., *Rotary Wing Structural Dynamics and Aeroelasticity*, AIAA Education Series, Washington, 1992.
[4] Bogoliubov, N.N. and Y.A. Mitropolski, *Asymptotic Methods in the Theory of Nonlinear Oscillations*, Gordon and Breach, New York, 1961.
[5] Brosens, P.J. and S.H. Crandall, Whirling of unsymmetrical rotors, *ASME J. Appl. Mech.*, **28** (1961) 355–362.
[6] Crespo da Silva, M.R.M. and D.H. Hodges, The role of computerized symbolic manipulation in rotorcraft dynamics analysis, *Comp. Math. Applications*, **12A** (1986) 161–172.
[7] Dimarogonas, A.D. and S.A. Paipetis, *Analytical Methods in Rotor Dynamics*, Applied Science Publishers, London and New York, 1983.
[8] Dugundji, J. and J.H. Wedell, Some analysis methods for rotating systems with periodic coefficients, *Am. Inst. Aero. Astr. J.*, **21** (1983) 890–897.
[9] Flashner, H., A point mapping study of dynamical systems. Ph.D. Dissertation, Department of Mechanical Engineering, University of California, Berkeley, 1979.
[10] Flashner, H. and C.S. Hsu, A study of nonlinear systems via the point mapping method, *Int. J. Num. Meth. Engg.*, **19** (1983) 185–215.
[11] Friedmann, P.P, C.E. Hammond and T.H. Woo, Efficient treatment of periodic systems with application to stability problems, *Int. J. Num. Meth. Engg.*, **11** (1977) 1117–1136.
[12] Friedmann, P.P., Numerical methods for determining the stability and response of periodic systems with applications to helicopter rotor dynamics and aeroelasticity, *Comp. Math. Appl.*, **12A** (1986) 131–148.
[13] Gaonkar, G.H., D.S. Simha Prasad and D. Sastry, On computing Floquet transition matrices of rotorcraft, *J. Am. Helicopter Soc.*, **26** (1981) 56–61.
[14] Gladwell, G.M.L. and C.W. Stammers, Predictions of the unstable regions of a reciprocal system governed by a set of linear equations with periodic coefficients, *J. Sound Vib.*, **8** (1968) 457–468.
[15] Guttalu, R.S. and H. Flashner, Analysis of bifurcation and stability of periodic systems using truncated point mappings, in *Nonlinear Dynamics: New Theoretical and Applied Results* (J. Awrejcewicz (Ed.)), 230–255, Akademie Verlag, Berlin, 1995.
[16] Guttalu, R.S. and H. Flashner, Stability analysis of periodic systems by truncated point mappings, *J. Sound Vib.*, **189** (1996) 33–54.

[17] Hsu, C.S., On nonlinear parametric excitation problems, *Adv. Appl. Mech.*, **17** (1977) 245–301.
[18] Hsu, C.S., On approximating a general linear periodic system. *J. Math. Anal. Appl.*, **45** (1974) 234–251.
[19] Johnson, W., *Helicopter Theory*, Princeton University Press, Princeton, 1980.
[20] Jury, E.I., *Inners and Stability of Dynamic Systems*, John Wiley, New York, 1974.
[21] Lindh, K.G. and P.W. Likins, Infinite determinant methods for stability analysis of periodic-coefficient differential equations. *Am. Inst. Aero. Astr. J.*, **8** (1970) 680–686.
[22] Nayfeh, A.H. and D.T. Mook, *Nonlinear Oscillations*, John Wiley, New York, 1979.
[23] Pandiyan, R. and S.C. Sinha, Analysis of time-periodic nonlinear dynamical systems undergoing bifurcations, *Nonlinear Dyn.*, **8** (1995) 21–43.
[24] Peters, D.A., Flap-lag stability of helicopter rotor blades in forward flight, *J. Am. Helicopter Soc.*, **20** (1975) 2–13.
[25] Poincaré, H., *Leas Methodes Nouvelles de la Mechanique Celeste*, Gautier-Villars, Paris, 1891.
[26] Poston, T. and I. Stewart, *Catastrophy Theory and its Applications*, Pitman Publishing, London, 1978.
[27] Sinha, S.C., D.-H. Wu, V. Juneja and P. Joseph, Analysis of dynamic systems with periodically varying parameters via Chebyshev polynomials, *ASME J. Vib. Acou.*, **115** (1993) 96–102.
[28] Shampine, L.F., *Numerical Solution of Ordinary Differential Equations*, Chapman & Hall, New York, 1994.
[29] Yakubovitch, V.A. and V.M. Starzhinski, *Linear Differential Equations with Periodic Coefficients*, Vols. I and II, John Wiley, New York, 1975.

Special Issue on
Singular Boundary Value Problems for Ordinary Differential Equations

Call for Papers

The purpose of this special issue is to study singular boundary value problems arising in differential equations and dynamical systems. Survey articles dealing with interactions between different fields, applications, and approaches of boundary value problems and singular problems are welcome.

This Special Issue will focus on any type of singularities that appear in the study of boundary value problems. It includes:

- Theory and methods
- Mathematical Models
- Engineering applications
- Biological applications
- Medical Applications
- Finance applications
- Numerical and simulation applications

Before submission authors should carefully read over the journal's Author Guidelines, which are located at http://www.hindawi.com/journals/bvp/guidelines.html. Authors should follow the Boundary Value Problems manuscript format described at the journal site http://www.hindawi.com/journals/bvp/. Articles published in this Special Issue shall be subject to a reduced Article Processing Charge of €200 per article. Prospective authors should submit an electronic copy of their complete manuscript through the journal Manuscript Tracking System at http://mts.hindawi.com/ according to the following timetable:

Manuscript Due	May 1, 2009
First Round of Reviews	August 1, 2009
Publication Date	November 1, 2009

Lead Guest Editor

Juan J. Nieto, Departamento de Análisis Matemático, Facultad de Matemáticas, Universidad de Santiago de Compostela, Santiago de Compostela 15782, Spain;
juanjose.nieto.roig@usc.es

Guest Editor

Donal O'Regan, Department of Mathematics, National University of Ireland, Galway, Ireland;
donal.oregan@nuigalway.ie